12-2006

INFLUENCE OF TEMPERATURE AND POLYMER/ MOLD SURFACE INTERACTIONS ON MICRO-FEATURE REPLICATION AT AMBIENT PRESSURE IN MICRO INJECTION MOLDING

Varun Thakur
Clemson University, vthakur@clemson.edu

INFLUENCE OF TEMPERATURE AND POLYMER/ MOLD SURFACE INTERACTIONS ON MICRO-FEATURE REPLICATION AT AMBIENT PRESSURE IN MICRO INJECTION MOLDING

A Thesis
Presented to
the Graduate School of
Clemson University

In Partial Fulfillment
of the Requirements for the Degree
Master of Science
Materials Science and Engineering

---

by
Varun Thakur
December 2006

Accepted by:
Dr. David C. Angstadt, Committee Chair
Dr. Igor Luzinov
Dr. Jian Luo

ABSTRACT

Microinjection molding is based on the concept of vario-thermal processing in which the injection unit heats the polymer and presses it into a micro featured mold. After the unit cools, the featured part is de-molded. An inherent problem with microinjection molding is poor feature replication. The polymer in the micro-cavity instantaneously freezes when it comes in contact with the mold wall thus, limiting the achievable aspect ratio of the features in the part.

This study assesses micro-feature replication at elevated mold temperature and ambient pressure using a variety of polymers and commonly used mold surfaces. In order to more fully explore the micro injection molding processing window, a better understanding of the interaction of polymer melt with the mold surface is needed. These interactions can be partially determined by measuring the contact angle of polymer melt directly onto the mold surface which can subsequently be correlated to the wetting and surface tension. Viscosity measurements provided a comparison of the behavior of different polymers to varying shear rates. Molding trials were performed on micro and nano featured mold surfaces at elevated mold temperatures and ambient pressure. Feature replication was analyzed quantitatively using an atomic force microscope, comparing the attained depth of the polymers for different aspect ratio features. A qualitative and dimensional analysis was also performed by field-emission scanning electron microscope. Crystallinity of the polymers in the molded parts was attained by X-ray diffractometer. While feature detail was well replicated for all the polymers, the moldings

exhibited poor dimensional accuracy due to high shrinkage in the parts. In general, polymers with low viscosity and crystallinity and a surface tension comparable to that of the mold material showed the best feature replication.

DEDICATION

I would like to dedicate this thesis and work to my dearest parents Dr. R.S. Verma and Mrs. Rajnish Prabha, my brother and my sister-in-law Dr. Manish Thakur and Dr. Mili Thakur; who have been a perpetual source of love, encouragement and motivation. This thesis would not have been possible without their support.

ACKNOWLEDGEMENTS

The successful completion of my Master's thesis was possible due to support and encouragement from several individuals. My deepest and sincerest gratitude to my advisor, Dr. Davd C. Angstadt, who helped me in developing my awareness and appreciation for the field of "Micro-Injection Molding". I thank you for all the guidance and support throughout my research efforts and thesis work.

My appreciation goes out to Dr. Igor Luzinov and Dr. Jian Luo for serving on my committee and guiding me throughout my research experience. Each of you was very instrumental in the completion of my thesis and in developing my overall knowledge in the field of Materials Science & Engineering.

I would sincerely like to thank Sahil Jalota for his endless help with SEM analysis and continual support. I would like to thank Dr. Douglas E. Hirt, Chemical Engineering Department and his group members for proving help in contact angle measurement. A special thanks to Mr. Amar Khumbar and Mr. Dayton Cash (EM Lab. Staff) for teaching me the operation of scanning electron microscope and helping me throughout the course of my thesis work. I really appreciate the help of Dr. Graham M. Harrison, Chemical Engineering Department and Deidra Cade, for the viscosity measurements. I would also like to thank Jake Jokisari for his help throughout the AFM measurements and Dr James E. Harriss for helping me with the cutting of Si wafers.

TABLE OF CONTENTS

Table of Contents (Continued)

LIST OF TABLES

LIST OF FIGURES

List of Figures (Continued)

Page

List of Figures (Continued)

Page

CHAPTER 1: INTRODUCTION

1.1 Micro-injection Molding Process

Polymer injection molding is an attractive manufacturing technique for many applications due to high productivity and the wide variety of shapes that can be produced [1]. It has been one of the most capable and cost effective techniques for mass production of small components. Benefits like reduced cycle times, high accuracy in large scale production for high aspect ratio microstructures have made it a well established process for polymer manufacturing [2]. Numerous studies have been conducted to produce accurate parts and enhance the micro molding process [1]. These enhanced micro-fabrication technologies can be divided into 2 groups, direct manufacture and replication techniques. In the direct techniques each polymer part is manufactured separately. These methods include laser ablation, cutting stereo-lithography and photo-lithography. In replication technique the polymer structures are replicated from a master mold. The most widely used technology in the industry is the process of polymer micro-molding [3, 4]. In the manufacturing industry micro injection parts typically have weight of less than 0.1 grams, wall thickness of less than 0.2 mm and contain even tinier holes, pins and channels [5]. The part tolerance range is typically in the micrometer range [6]. Generally, parts having features at or below these specifications are considered micro molded components.

1.2 Applications

The significance of micro-molded parts can be easily predicted by the extent of their wide range of applications. The applications of the parts include electrical,

electronics, computers, medical, and biotechnological devices [5]. Micro-fabrications of polymer are becoming increasingly important and considered as a low-cost alternative to the silicon or glass-based Micro-electro-mechanical-system (MEMS) technologies [7]. Polymeric micro lenses play an important role in reducing the size, weight, and cost of optical data storage and optical communication systems as shown in Fig 1 [8, 9]. Newer medical technologies are driving further development of smaller plastic components. The market of health care product relies heavily on micro-scaled mechanical, analytical and fluidic polymer components [6]. The most widely used applications of micro molded parts are the compact and digital versatile disks CDs and DVDs. These are made by the injection compression molding of Polycarbonate with a molding cycle time of less than 5 seconds [9]. These disks have parallel grooved features having dimensions of 0.3 μm by 0.5 μm with a spacing of 0.16 μm as shown in Fig 2 [10, 11]. In order to meet the increasing demand for smaller components like nano-electro-mechanical-system circuits, considerable improvement of the current micro injection molding process is desired. Micro molding of polymers is performed in many forms. All these processes are based on the concept of vario-thermal processing technique. Vario-thermal processing involves heating the cavity before injection of the polymer and cooling down before demolding [12]. This process facilitates the molding and demolding of the components.

1.3 Types of Molding Techniques

A brief review of commonly adopted micro molding techniques is given below.

1. Micro Injection Molding: In this process an injection unit heats up the polymer and injects it under high pressure into a heated mold equipped with micro structured tools and mold inserts. Polymer is then cooled and de-molded [4, 13].

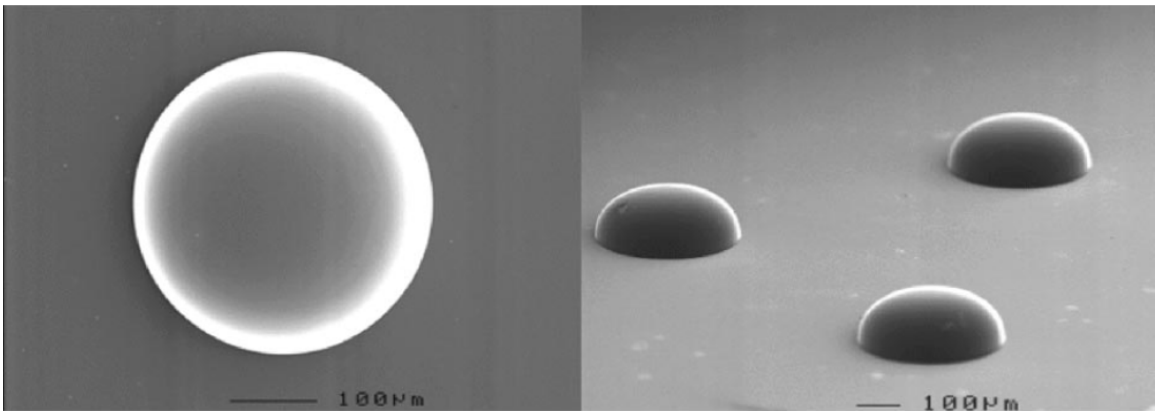

Figure 1 Micro-molded micro-lens for optical applications [8].

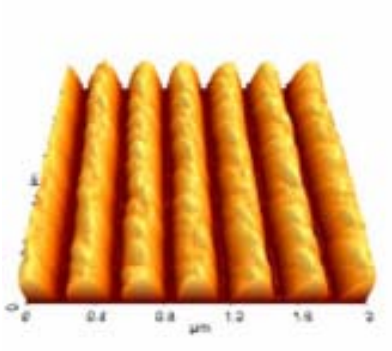

Figure 2 Micrograph of a CD master mold obtained from Atomic Force Microscope [14].

2. Reaction Injection Molding: Two polymeric components a pre-polymer, a curing agent are injected in molding tool and are cured with thermal initiation or UV-curing [2, 4].
3. Hot Embossing: A polymer sheet at an elevated temperature is compressed by mold tooling and inserted into a vacuum to replicate the surface features on the sheet [15].
4. Injection Compression Molding: The plasticized polymer is injected in a semi closed tool and then fully pressed to give it a final shape. Demolding in this process is much easier than the other techniques [4].
5. Thermoforming: In this process a film or sheet is molded to a tool with micro structure on one side. It is then heated up and pressed to the feature by vacuum or hot pressurized gas [4].

Out of these, the most popular and widely studied are the techniques of micro-injection molding and hot embossing. Injection molding techniques are used in industry for fabrication of most of industrial plastic components and are preferred over hot embossing where structures are not complicated and have low aspect ratios. Micro-injection molding techniques have much shorter cycle times for mass production [3]. Hot embossing is used only for a selected few optical applications where high precision and quality and low levels of molecular orientations are required [15].

However, in micro scale molding, factors that have negligible effect in conventional injection molding play an important role. Interfacial effects like surface tension, heat transfer and surface roughness of the mold material play a vital role at micro scale [9]. As the walls of the molded parts become thinner surface properties of the

feature and part dimension become largely dependent on irregularities, scale of roughness on mold surface and molding conditions [5].

1.4 Drawbacks

Micro-injection molding suffers from inherent problems of poor feature replication and limitations regarding the aspect ratio that can be achieved with small mold inserts. The micro-scale fabrication has large surface area to volume ratio thus interfacial factors such as wettability, friction and adhesion between polymer and tooling becomes critical [16]. The polymer in the micro-cavity instantaneously freezes when it comes in contact with the mold wall. This problem is exaggerated in very small feature replication [17]. Better understanding of the interaction and impact of interfacial effects due to wetting of mold by the polymer is required to eliminate these drawbacks. In micro-molding, properties like surface tension and viscosity play a critical role in the overall effectiveness of the process. The study of this interaction of polymers with mold material with respect to interfacial effects has been very limited in the past. Strong interaction implies good feature replication but difficulty in demolding. Weak interaction hinders good feature replication. Thus, optimization of these conditions is very critical for the overall success of the process.

The work presented tries to identify this impact of interfacial effects on feature replication due to wetting of the mold by polymer melt under low processing pressure conditions. It is mainly the complex interplay of rheological and thermal effects at extremely short time scales, which makes it difficult to analyze and understand the problem [18]. To quantify the interfacial effects, in this study two important parameters (a) contact angle and (b) surface tension are examined [16, 19, 20].

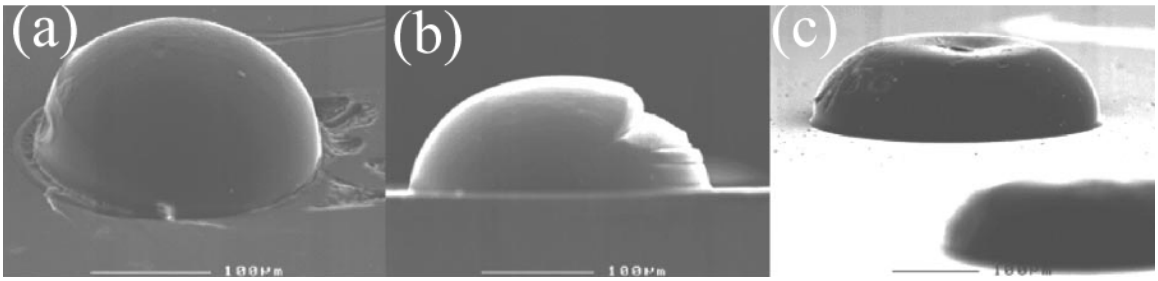

(i)

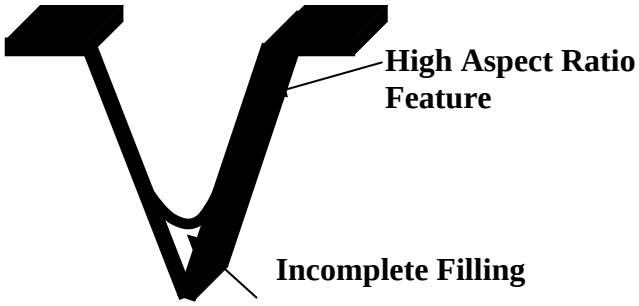

(ii)

Figure 3 (i) Molding defect in a microlens (a) slip (b) burst (c) shrinkage [8].
(ii) Schematic representation of incomplete filling caused due to premature freezing in high aspect ratio features.

A high mold surface temperature is typically a precondition for the accurate reproduction of the features [21]. Normally, the injection molding process is carried out at relatively low mold temperatures (less than Tg of polymer) and very high pressures.

This necessitates the attachment of heavy pressure equipment with the device. The micro molding process has to be carried out with big and bulky machines. This is detrimental to the sensitivity of the process in which inefficient dissipation of heat can be a critical factor. Due to the large size of equipment the mold is not able to heat and cool rapidly causing incomplete filling of mold and poor feature replication. With ever diminishing part volume and shot size, conventional molding machines are no longer feasible for the micro molding process [22].

In this study the feasibility of one end of polymer processing window by micro injection molding is studied. Features are molded with the use high temperature and ambient pressure conditions. If effective feature replication is possible by this method of processing then it may be possible to make smaller molds as well as machines. This would help in heating up of the molds faster and thus achieve a faster variotherm process. Low pressures and high temperatures will also reduce the surface defects caused by uneven distribution of heat and polymer flow in the conventional micro injection molding process [23]. Other benefits of low pressure application will include significant reduction of the clamp force tonnage requirement, less expensive mold and presses and lower stresses in mold and parts [22].

1.5 Contact Angle and Wettability

(a) Equilibrium Contact Angle

When a drop is placed on a solid surface the difference in the surface tension of liquid and the surface causes it to form a definite angle θ between the liquid and the solid phases. If the same liquid is placed on surface of increasing surface energy, the contact angle decreases as the surface energy of solid increases. Finally, complete wetting (θ=0º) occurs if the surface tension of the liquid is smaller than the surface tension of the solid [24]. This surface tension at which the liquid exhibits a zero contact angle on the solid is called critical surface tension [25]. Contact angle is governed by the force balance at this three-phase boundary and is defined by Young's Equation.

$$\gamma_{lv}\cos\theta = \gamma_{sv} - \gamma_{sl} \quad \text{...Equation (1)}$$

Where, γ_{lv} is surface tension of the liquid in equilibrium with its saturated vapor, γ_{sv} is surface tension of solid in equilibrium with the saturated vapor of the liquid and γ_{sl} is the surface tension between the solid and the liquid [25-27].

Stable equilibrium is obtained when following condition are satisfied:

1. The surface is rigid and immobile.
2. The surface is smooth.
3. The surface is compositionally homogenous.
4. There are no interactions between the liquid and the solid surface [27].

Most of these conditions are not very often met when dealing with polymers so contact angle hysteresis is observed. γ_{sv} in equation 1 is not the actual surface tension of the solid (γ_s) but represents the surface tension of the solid resulting from adsorption of

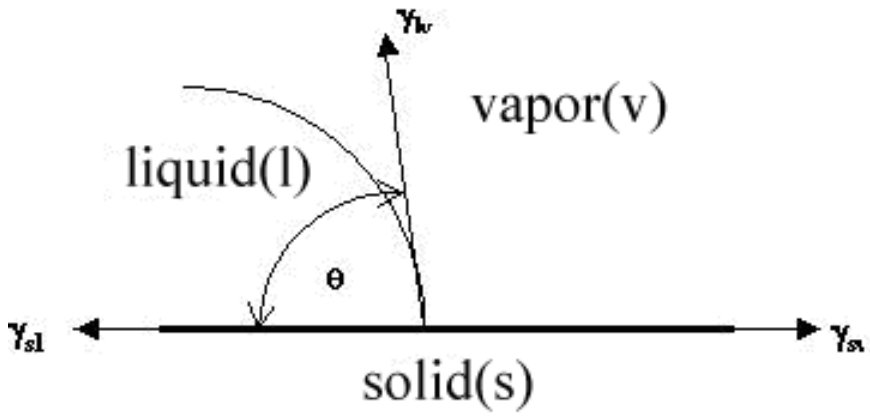

Figure 4 Forces on a drop placed in equilibrium on a flat surface (Equilibrium Contact Angle) [26].

vapor form a liquid. The amount of reduction observed in the actual surface tension of the solid γ_s caused by the absorption of vapors is referred to as spreading pressure Π_s [25].

Where, $$\Pi_s = \gamma_s - \gamma_{sv}$$ …Equation (2)

Also, contact angle in terms of spreading pressure would be [25],

$$\cos\theta = \frac{\gamma_s - \Pi_s - \gamma_{sl}}{\gamma_{lv}}$$ …Equation (3)

In terms of critical surface tension γ_c, the spreading pressure is defined as [25],

$$\begin{aligned}\gamma_c &= \lim_{\theta \to 0} \gamma_{lv} \\ &= \gamma_s - \gamma_{sl} - \Pi_s\end{aligned}$$ …Equation (4)

The contact angle decreases as surface tension of the solid is increased for the same liquid [24, 25]. The interaction of the surface and polymer can also be studied through the work of adhesion. It is defined as the reversible work required in separating two bulk phases from their equilibrium separation to infinity. The better the adhesion, the better is polymer replication [25].

Thus work of adhesion W_a is given in equation 5 [25],

$$W_a = \gamma_{SV} + \gamma_{LV} - \gamma_{SL}$$ …Equation (5)

This implies that high surface energy solids will have better wettability and thus can be used as efficient mold materials for injection molding. Similarly polymers with lower surface energy at processing temperature will produce better feature replication. But the interfacial tension with the polymer should be kept low to avoid problems in de-molding.

There are two types of contact angles, static and dynamic. Static contact angle, as the name suggests, is measured when the system is stationary. It is determined after the equilibrium of interfacial tensions is formed at a stationary liquid front. Dynamic contact

angles are determined when either the system or liquid front is in motion. It is determined by a balance of the interfacial driving force and viscous retarding force. Dynamic contact angles are usually dependent of rate.

The contact angle depends entirely upon how the melt interacts with the surface. Thus the measure of contact angle of a polymer on a surface gives a fair idea of the interaction and wettability of the polymer melt with the surface. The understanding of this interaction can be very useful in enhancing the efficiency of micro injection molding process where interaction of tooling takes place with the polymer melt during the filling process [28].

(b) Methods for measuring contact angle and surface tension

Polymers when in liquid state have high viscosities and thus long relaxation times so they become fluid only at high temperatures [29]. This combination of viscosity and relaxation time makes the conventional experimental methods for determining contact angle and surface tension difficult. Most methods require long time for equilibration and the thermal stability of polymers at high temperature also restricts surface tension measurements of many polymers [29, 30]. Thus the measurement of interfacial tension on solid surfaces becomes difficult because of the experimental difficulties caused by high viscosity, limited thermo-stability and high measuring temperatures [30, 31].

The most common techniques for the measurement for both interfacial and surface tension are classified as the drop shape method [32]. Drop shape methods are commonly used to measure surface tension in stable systems having nearly equilibrium conditions. The shape is governed primarily by surface tension and gravity. In principle when gravitational and surface tension forces are comparable drop shape methods can be

effectively used to determine surface tension. Drop shape methods have simple yet versatile mechanics [31, 33]. The Axi-symmetric Drop Shape Analysis (ADSA) is used in most cases as a pendant drop method to determine the surface tension of the polymer melts. In this method a drop is suspended from the tip of a capillary. The shape of this experimental drop is fitted to a theoretical drop profile according to Laplace equation (Equation 6) of capillarity. ADSA includes local gravity, the densities between the liquid phases, and several coordinate points along the drop surface [31-34].

$$\Delta P = \gamma\left(\frac{1}{R_1}+\frac{1}{R_2}\right) \qquad \text{...Equation (6)}$$

Where γ is interfacial tension; R_1 and R_2 are the principal radii of curvature of drop; and ΔP is pressure difference across the curved interface

In the sessile drop method, a liquid drop is placed on a horizontal solid surface so that the edge of the drop and its reflected image are both visible when viewed in cross section through a microscope. This allows the tangent to be determined at the point of contact between the drop and the surface, which allows the calculation of the surface tension using equation 1. This is the most commonly used method of measuring contact angle in many systems [35, 36]. The drop profile can also be fitted with Laplace Equation as in case of pendant drop method. Drop analysis methods usually require an equilibrium state of the melt droplet. This implies that high viscosity, high temperatures and long annealing times are necessary to achieve equilibrium for measurement of contact angle. As a result most of the thermally instable polymers and heterogeneous structures cannot be studied. In this case the measured value is not the surface tension of the whole material but is governed by the surface properties of droplet. Surface tension of polymers

like High Density Polyethylene cannot be measured by Pendant Drop Analysis because of high viscosity and high elasticity [34].

Neumann and co-workers [35, 37, 38] made a modification in the sessile drop method. A small hole was made in the flat solid sample and a small drop is formed on top of this hole. The size of the drop was then increased by feeding liquid to the drop from below the solid surface by a syringe. This procedure prevented the drop from oscillating and destroying the axis of symmetry.

The Wilhelmy-capillary rise method eliminates this drop size effects on contact angle measurements. In this method a solid plate or fiber is immersed vertically into a liquid and held in a vertical position by an electro-balance. The contact angle determination is done from the capillary rise at a vertical plate when the plate is stationary for static angles. Dynamic contact angles are measured when the plate is moving. The detail of the process is shown in Figure 5.

The contact angle can then be calculated from the measurement of the capillary rise by a cathetometer or eletrobalance which records the total wetting tension on the plate as [39].

$$\gamma_l \cos\theta = \frac{F}{P} \qquad \text{...Equation (7)}$$

The main drawbacks of the Whilhelmy plate is the buoyancy correction that has to be made. The surface tension is not measured directly. The measured quantity is the wetting tension $\gamma_l \cos\theta$, complete wetting of the fiber by the polymer melt (contact angle $\theta=0°$) is required to obtain the surface tension γ_l [31]. This method also requires knowledge of the density difference between the liquid and the vapor, the liquid surface tension, and the acceleration due to gravity [28, 35, 37, 38, 40, 41].

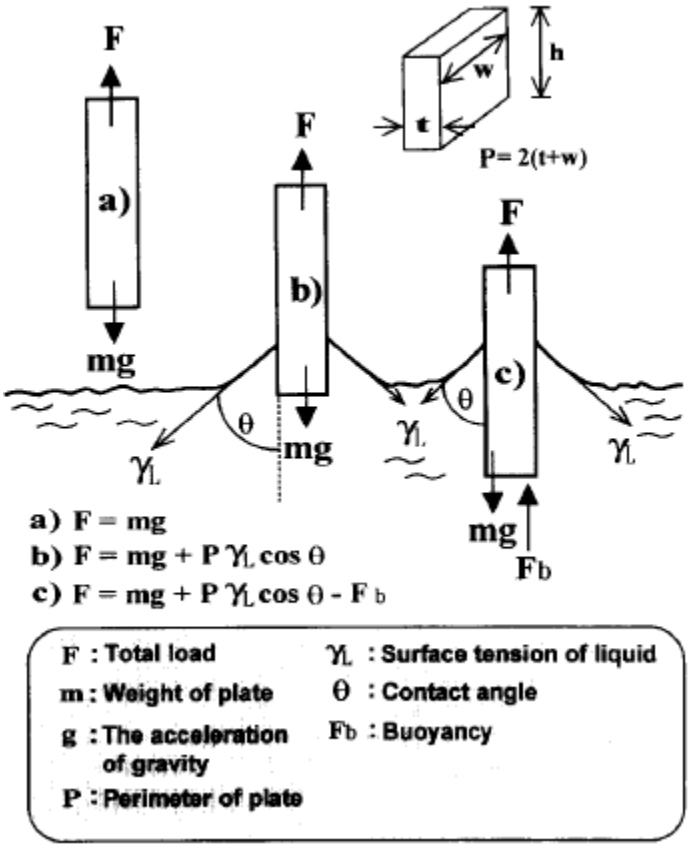

Figure 5 Principle of contact angle measurement by Wilhelmy Method [39].

In the inclined plane method, the solid sample is placed on a motor-driven inclined plane. When the plane of the solid surface reaches a critical slope, the drop starts to slide. The measured angle at the downhill edge of the drop approaches $\tilde{o}$a, and the angle at the uphill edge approaches $\tilde{o}$r. The angles should be measured immediately prior to the drop starts to slide [35, 41-49]. The thesis will involve measurement of static contact angle and viscosity of each studied polymer over a range of temperature corresponding with the processing temperature of polymers. This will give us a fair idea about the surface energy of polymer melt and its behavior at the temperature of operation.

(c) Prerequisites for measuring equilibrium contact angle

1. In a drop there always exists a positive line tension which provides a driving force for the drop to shrink in the lateral direction, thereby increasing the contact angle from the value predicted by the Young's Equation [50]**.** Smaller drops give smaller values of the pseudo line tension, with magnitudes as low as 10^{-3} dyne observed for drops with diameters less than 0.1 mm [50-52]. For this reason the smallest possible drops should be used for contact angle measurements as smaller drops have contact angles which more closely approximate the equilibrium values.

2. For ideal surfaces, which are considered to be rigid, smooth (i.e., surface roughness << 0.5 μm), and chemically homogeneous, there exists only one equilibrium contact angle [53-55]. For real surfaces which are considered to be rough, heterogeneous, and/or non-rigid, there may be several observed contact angles, which results in contact angle hysteresis [53, 56]. As seen earlier Equation 1 relates the interfacial tension between a solid and a liquid (γ_{sl}) to the solid surface tension (γ_s), the liquid surface tension (γ_l), and the contact angle (θ) on an ideal horizontal surface [53, 57]. It has been

shown that the advancing contact angle is less sensitive to surface roughness and heterogeneity than the receding angle. Therefore, advancing angle data are commonly used to calculate surface and interfacial tension components [53].

Usually when a polymer drop is placed on the metal surface it does not show an equilibrium contact angle. In fact, it is observed that the drop spreads until it attains a zero contact angle with the surface. The rate of this polymer spreading can be correlated to the wetting abilities of the polymer. Therefore, for studying the relationship of the polymer liquid spreading behavior a sessile drop having very low volume has been taken.

1.6 Prior Studies on Spreading of Polymers on Surfaces

There have been many attempts to study the flow of liquids on solid surfaces hence highlighting the importance of interfacial effects. Schonhorn et al. [58] studied the kinetics of wetting of high and low energy surfaces by some polymers. The rate of approach of the apparent contact angle to its equilibrium value and the change of the radius of its base was studied as a spreading parameter. Silberzan [59] studied differences in the spreading behavior of high molecular weight and low molecular weight polymers on high energy surfaces with the help of optical microscopy and ellipsometry. It was observed that high molecular weight polymers had a slower spreading rate than the low molecular weight polymers on the same kind of surfaces. Bruisma [60] studied the slow spreading of polymers on different surfaces. It was found that the spreading velocity is not dependent on the difference in surface energy of a wet and a dry surface.

The spreading of a polymer on a surface depends on a spreading pressure given by

$$S = \gamma_{sv} - \gamma_{sl} - \gamma \qquad \text{....Equation (8)}$$

where, γ_{sv} per unit area of the dry substrate**;** γ_{sl} interface energy between liquid and substrate; and γ the actual surface tension. A positive value for S (wetting) is a necessary condition for spreading. For negative S (non-wetting), the contact angle is determined by equation 1.

Rogers et al. [61] attempted to determine a suitable polymer and clay coating for synthesis of nano-composites through direct contact angle measurements of polymer melt. In experiment a 1mm diameter polymer particle was heated in a chamber and allowed to melt slowly. The shape was recorded after every 30 seconds for a period of four hours. Their study found that the polymers showing complete wetting were more suitable for the nano-composites. Although this study was not directly related to microinjection molding it gives a fair idea as to how direct polymer melt contact angle measurements are suitable for studying the wetting behavior of polymers on surfaces.

Wouters [62] used a conventional contact angle microscope along with a goniometer to study polymers spreading on surfaces with viscosity effects to see the spreading of powder coatings on surfaces. The wetting and leveling process that occurs during film formation is determined by a balance of the surface tension (driving force) and the viscosity (resistance).

It was inferred that lower surface tension facilitates the substrate wetting process, but if it is too low leveling is poor, resulting in wavy surfaces. A higher surface tension promotes leveling, but if it is too high the wetting is poor, resulting in crater defects. For best flow characteristics, the surface tension of the system should be as high as possible, and the melt viscosity as low as possible [62]. As can be seen in Figure 6, low surface tension and/or high melt viscosity will stop the film flow-out, leading to a poor film flow.

Cratering during the film formation restricts the upper value of the surface tension, while low melt viscosity may lead to poor physical storage stability [62]. Thus, melt viscosity is a critical factor in achieving proper spreading and replication of a melt on a surface. The lower the melt viscosity the better is the feature replication if the polymer has ambient surface tension.

1.7 Prior Studies on Improvement of Micro Molding

None of these studies mentioned have directly addressed effects on polymer processing by injection molding. In fact very few works have been conducted that directly study the polymer/mold interfacial effects in relation to micro molding. Yoon et al [14], investigated the replication quality and durability of the mold surfaces for nano scaled features, using electroformed nickel based DVD mold and Si mold inserts. AFM was used to study the replication quality of compression and injection molded polymers. Although it was a good initial attempt to study the effect of mold surface on replication, no quantification of the polymer/surface interaction was made in form of contact angle or wettability measurements. Choice of surfaces as well as polymers was also limited.

Srirojpinyo et al. [9] carried out with the previous work of Yoon and studied the effect of melt temperature ,injection velocity and packing pressure on the depth ratio and surface quality of the molded part. Interaction of four polymers was studies with a nickel based DVD master mold. It was proposed that high melt and mold temperatures, rapid injection and higher pack pressure produced the best nano-scale feature replication. Here also no direct data on wettability measurements were reported. It was seen that feature replication was mainly affected by interaction between tooling surface and polymer melt. The choice of mold material was also narrow.

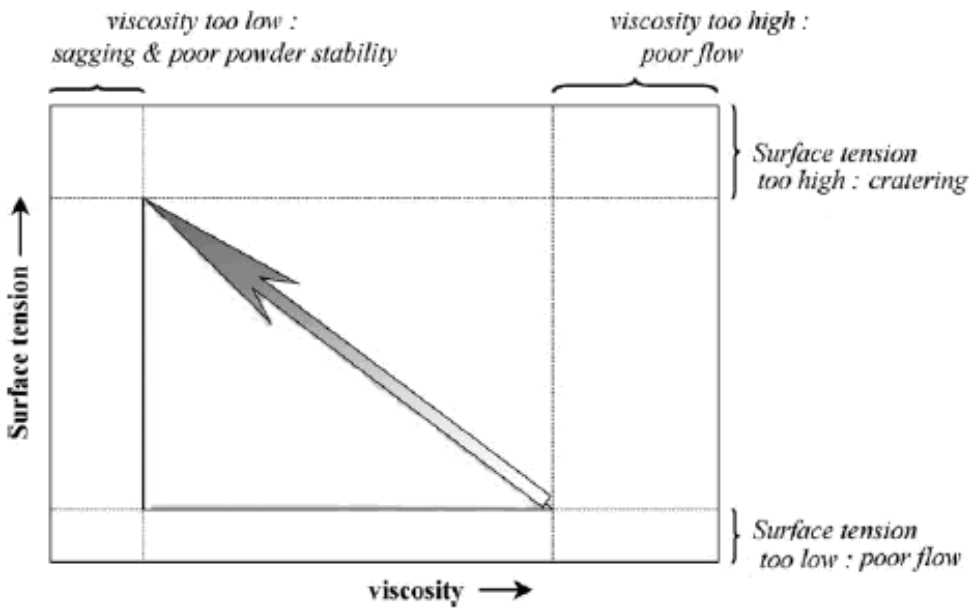

Figure 6 Influence of the magnitude of melt viscosity and surface tension on the polymer film spreading [62].

Srirojpinyo et al. [16] further modified their approach and part replication was correlated with contact angle measurements which were qualitatively converted to wetting and surface tension. The contact angle and the sliding angle were measured for multiple polymers and surfaces. It was found that the polymer melts exhibiting higher wettability with respect to the insert tool materials and mold surface provided better feature replication. Note that the contact angle was measured using reference liquids on the solid surfaces as well as on solid polymer films in lieu of direct measurements of polymer melt contact angles. This study did not take into account the change in the polymer surface tension with increased in temperature which could change the interfacial tension calculated by reference liquids.

Simulation tools appropriate for micro scale polymer processing have been used by Majumdar et al. [5]. This study compared micro-molded parts produced from two materials over a range of processing conditions were corresponding with results of filling simulations. Molded parts were studied with respect to fill pressures; weld line strength and relative shear stresses developed in the parts. The results at high pressures were consistent with experimental trends but no correlation could be made between breaking strength temperature at the weld line and shear stresses.

Michaeli [63] treated the inlay mold parts material with plasma and analyzed whether it was possible to predict bonding strength of hybrid components from wetting measurements. Measurements of polymer melts using pendant drop was not feasible so different test fluids were used on solid surfaces to calculate surface tension much like that used by Srirojpinyo. Tests inferred that prediction of adhesiveness by wetting tests was not a reliable method, possibly due to the use of reference liquids instead of the actual

polymer melt. Chen et al. [64] studied how rapid mold surface temperature control and different heating rates coupled with surface coating could reduce the defects on the surface of ABS micro-featured parts produced by injection molding. The study did not directly address mold/polymer interaction but provided insight on what type of heating, heating rate and coatings can help improve feature replication and reduce defects.

In most of the above mentioned studies, the surface energy was studied with respect to reference liquids and then compared with the replication quality of molded surfaces. This method cannot be feasible because surface tension of polymers decrease as the temperature is increased [25]. Thus, the melt processing temperature surface energy is very different from the polymer solid surfaces on which these reference liquids are measured.

Out of the many attempts to improve the micro injection molding technology the one most pertinent to our study was the Rapid Thermal Mold Design (RTR) technique. RTR process has been successfully applied to injection molding technology. In this process, rapid increase in the temperature of the mold is achieved through induction heating. Through this the problem of premature freezing was countered and attainment of large aspect ratio was possible [65]. Use of RTR technology also reduced the total cycle time due to the low thermal mass involved [66]. Although RTR technology has shown promising ability to replicate features on micro and nano-scale, there are potential drawbacks of the technology. One of the primary concerns is the low mold life and dimensional accuracy of the replicated features. Rapid heating and cooling results in thermally induced stresses in the mold, which leads to reduced mold life. This result in shorter mold setup replacement cycle time and thus increases the cost. RTR also causes

large mold surface deflections due to high thermal gradients. This also affects the replication precision of the application [67].

In this thesis the optimization of the feature replication is approached only through the application of high mold temperatures. This will give us an estimate of the extent of feature replication at one extreme end of the micro injection molding process window. The feasibility of the process, the factors affecting the process and the part quality produced in analyzed for the further development of the micro injection molding process. The success of this approach will further introduce additional design freedom, new application areas, unique geometrical features and improved material and part properties in the micro injection molding process.

CHAPTER 2: MATERIALS AND METHODS

2.1 Materials

(a) Polymers

In this study, four different polymers were selected depending on the structure and general properties suited for micro injection molding. The polymers chosen varied in the degree of crystallinity. Polystyrene (PS) and Poly (methyl methaacrylate) (PMMA) were the amorphous polymers exhibiting high transparency and similar flow properties. Polypropylene (PP) was semi-crystalline in nature, largely used as a commodity polymer with good mechanical properties. High Density Polyethylene (HDPE) was the most crystalline polymer out of the four polymers used and had the highest visco-elastic properties. These polymers provided an examination of the effect of different characteristics of polymers on the part produced. All the polymers were injection grade (TDL plastics, Texas, U.S.A.) and their properties are mentioned in Table 1(a) as provided by the manufacturer. General polymer properties are given in Table 1 (b).

Table 1 (a) Properties of polymers used in the study

Polymer	Structure	MFI (g/10 min)	Tensile Modulus(GPa)
HDPE	Semi-Crystalline	12	1.28
PP	Semi-Crystalline	11	1.03
PS	Amorphous	9	3.03
PMMA	Amorphous	15	3.10

Table 1 (b) Properties of polymers used in the study [68, 69]

Polymer	Density Amorphous(g/cc)	Density Crystalline(g/cc)	α_g X 10^{-4} K^{-1}	α_r X 10^{-4} K^{-1}
HDPE	0.855	1.00	7.1	13.5
PP	0.85	0.95	-	-
PS	1.05	-	2.0	5.5
PMMA	1.17	-	2.6	5.1

(b) Tool Material

The characterization of the polymers was done on four different materials used as tooling, molds and mold inserts in the micro injection molding process. The surfaces used as mold were oil-quenched Tool Steel (TS), Stainless Steel Grade 304 (SS), Aluminium T-651 alloy (Al) (Metal Supermarkets, Columbia, SC, U.S.A and the most commonly used mold insert in micro injection molding in form of silicon (Si) wafer (Lehigh University, Bethlehem, PA, U.S.A.). These materials differed in surface energy, durability and ability to withstand high temperatures. The common material properties include ease of fabrication of features on them, durability and sufficient hardness to withstand high pressure and temperature. In this study, the behavior of polymer was studied with respect to the different spreading rates and interaction with each of these surfaces.

2.2 Characterization of Polymers

(a) Differential Scanning Calorimetry (DSC)

In order to choose a suitable temperature for operation/handling of polymers, differential scanning calorimetry (DSC) measurements were performed on all of them. The glass transition temperature (T_g) and melt temperature (T_m) was found out from the

DSC data curves. The DSC measurements were taken in a helium atmosphere at a heating rate of 20° per minute.

(b) Rate of spreading measurements

When a polymer melt droplet is placed on a metal surface at high temperature the polymer starts to spread due to high surface energy of the metal surface. Due to the difference in surface properties of metals and polymers the spreading rate is different for different sets of surface/polymer. Thus, measurement of change in contact angle of a polymer on a particular metal surface helps to quantify the spreading rate of different polymers that can be directly related to the wettability. This rate of spreading can be quantified by calculating the change of contact angle of polymers on mold surface with time. Contact angle measurements were performed for the four polymers on the four surfaces of the study. The surfaces of the metals were thoroughly cleaned prior to use with acetone and distilled water to eliminate any impurities on the surface. Prior to that, the surfaces were polished to get their surface roughness below (Ra) 0.5 microns which was monitored by a TR100 Surface Roughness tester.

The contact angle variation as a function of time was studied by a contact angle goniometer (G10, Kruss, Hamburg). Calibration of the software was performed prior to start of each run. Typically, a polymer bead having constant weight of 0.02 grams was taken for each measurement to eliminate any variability caused by difference in weight of the polymer. The apparatus consisted of a heated chamber containing a quartz window for observation. The cleaned surface and polymer pellet was placed in the chamber and preheated to bring the surface of tool material and polymer in thermal equilibrium for 9 mins as shown in Table 2. The whole chamber was then heated at a rate of 1°C per

minute till temperatures shown in Table 2 were reached for respective polymers. The temperature was deliberately taken well above the melting points of the polymer to make them wet the surface appreciably. After incubating, the drop of polymer was formed on the surface. The pictures of changes occurring in the drop were collected at an interval of 5 seconds using a CCD camera attached to the chamber. The chamber was purged with nitrogen in order to avoid the degradation of polymers during contact angle measurements. The drop shape analysis (DSA) program software attached to the G 10 Kruss instrument fitted the profile of the drop formed and calculated the value of contact angle for the sessile drop. The contact angle was determined from the angle made between the baseline representing the flat mold surface and the tangent to the surface curvature. The contact angle measurements were manually confirmed by measuring the height (h) and base (l) of the drop from the photograph collected by the CCD camera. The drop and bubble method formula was used and is given as equation 9.

$$\theta = 2\tan^{-1}\sqrt{\frac{2h}{l}} \qquad \text{…Equation (9)}$$

where, θ is the contact angle of the polymer drop.

As soon as the polymer melts it begins to spread on the surface thereby, decreasing the contact angle exhibited. The rate of decrease is very rapid initially but becomes slow after some time. Similar to the injection molding process the feature replication takes place in the initial period of the process, the measurements of the contact angle from the drop are taken for a period of 5 minutes. The behavior of the polymer with the surface is studied for this initial time. The initial temperatures used for this contact angle measurement are shown in second column of Table 2. To see the change in rate of spreading with the increase in temperature a second set of temperatures

were used. The spreading rate was monitored after increasing temperature by 15ºC from the previous set. Similar steps were executed for the contact angle measurement as in the first case, that is, measurements were taken after every 5 seconds from the image of the sessile drop. These temperatures are shown in third column of Table 2.

Table 2 Analysis of polymers (a) low temperature (set 1), (b) high temperature (set 2)

Polymer	Time of pre-heating (mins)	Temperature of pre-heating (ºC)	Low temperature CA (ºC, SET 1)	High temperature CA (ºC, SET 2)
HDPE	9	130	145	160
PP	9	160	185	200
PS	9	205	220	235
PMMA	9	225	240	255

(c) Viscosity measurements

The melt viscosity of the polymer was measured using an Advanced Capillary Extrusion Rheometer Acer 2000. The polymer was placed in a steel cylinder and heated to the temperature of analysis. The viscous polymer was then forced through a die of known diameter by a rotating ram. The volume of polymer flowing per unit time is used to find the apparent shear rate γ_a. The readings were taken only after the velocity of the polymer extruded through the die is constant. The apparent shear stress σ_a was measured by a transducer placed just near the die entrance. A die with length to diameter ratio (L/D) of 10 was used with a transducer of 75 MPa.

Apparent viscosity is given as

$$\eta_a = \sigma_{a/} \gamma_a \qquad \text{...Equation (10)}$$

The shear rates ranging from 10 sec^{-1} to 10000 sec^{-1} were applied to get a flow rate profile of the polymer. The change in the corresponding viscosity of the polymer was

plotted with respect to the change in shear stress. The plots gave us direct comparison of viscosity of different polymers at different (a) shear rates, and (b) temperatures. The polymers usually show a non Newtonian flow after a certain shear rate and thus obey Power law fluid laws. The Power law fluids can be described by Ostwald-deWaele-Nuttingas for the fluids that obey the relation in equation 11:

$$\eta = m\dot{\gamma}^{n-1} \qquad \text{…Equation (11)}$$

where η is the viscosity; $\dot{\gamma}$ is shear rate; and n is the power law index.

For n less than one, the fluids are called pseudo-plastics. The power law predicts that the effective viscosity would decrease with increasing shear rate indefinitely, requiring a fluid to have infinite viscosity at rest and zero viscosity as the shear rate approaches infinity. It was observed that most of the polymers were power law fluids above a certain shear rate. The exponent n can be found from the log-log plot of shear rate versus viscosity. This way a direct comparison is obtained as to which polymer shows the maximum fluctuation in viscosity with shear rate as well as with the increase in temperature. The viscosity measurements were performed for temperature set 1 and 2 as shown in Table 2.

2.3 Mold Feature Preparation

2 different sized features are examined in this study; (1) parts molded from micro-featured dimensioned surfaces with dimensions ranging in a few hundred microns, and (2) nano-featured parts with dimension ranging up to a few hundred nanometers. Micro-features were formed on Stainless Steel (SS). Nano-features were created on silicon (Si) wafers (Lehigh University, Bethlehem, PA, U.S.A.).

For creating micro-features on the tool materials, a Wire Electric Discharge Machining (EDM) process was employed. In this process, features are made by rapidly removing the material with a recurring electric discharge applied in the presence of an electric field between an electrode used as cutting tool and the tool material. The electrode is guided in order to obtain the desired shape. A series of consecutive sparks removes the material and creates the micro-features on the surface. The surface of the tool material is not smooth as craters and depressions are formed due to the sparks produced. The feature was formed in the shape of grooves and elevations running parallel along the length of the whole surface. The sparks from the EDM process also caused very small dimples/craters on the surface. The features formed had semi-circular grooves with radius of 177 μm, whereas the distance between midpoints of rounded grooves was 406μm. This feature is shown in the SEM micrograph of Fig 7a. The craters formed from the sparks can be seen visually in this micrograph. Since these features are an order of magnitude smaller than the groove dimensions, they provide a qualitative measure of the replication of the polymers after molding is performed.

Nano-features were developed by Deep Reactive Ion Etching (DRIE) on silicon wafer, which was performed at Lehigh University. A modified Bosch process of DRIE was adopted to achieve nearly vertical structures. This process required a highly reactive gas, sulfur hexafluoride (SF_6) to perform a nearly isotropic etch of the substrate. Afterwards a PMMA layer was developed on the surface, which protected the substrate from further chemical attack and prevented further etching. The last step in this process was plasma etching of prepared PMMA-masked Si-wafer. In this step, the piece was

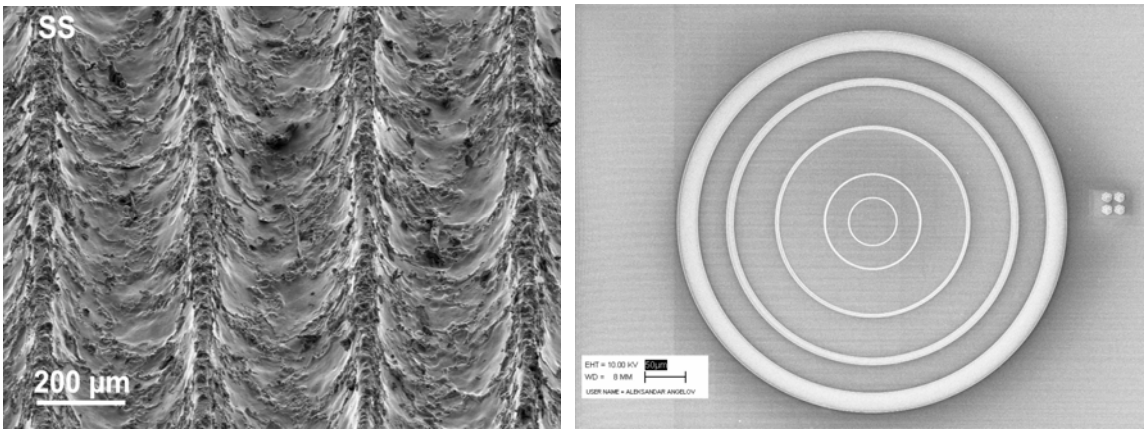

Figure 7 Tool materials (a) stainless steel material having micro-featured surface, and (b) Si-wafer having nano-featured surface consisting of 5 concentric rings of varying diameter

placed in a chamber that produces collimated stream of ions that bombard the substrate. This process helped to remove thepassivated layer from the surfaces of the previously etched trench. This process however, does not remove the passivated layer from the sides. Therefore, this etching process on a whole acted preferentially in the vertical direction. Thus, desired features are formed. These etch/deposit steps are repeated many times. The nano-structure formed consisted of five concentric rings having varying widths and depths (Fig 7b). The aspect ratio (aspect ratio=depth/width) ranged from 0.5 to .01 in the different rings of the feature. This helped in examining the replication behavior with different polymers at varying aspect ratios. The depth of each ring was kept constant at approximately 400 nm whereas the widths of each ring are about 25 micro (Ring-4 outer most ring), 8 microns (Ring-3), 3.5 microns (Ring-2), 1.5 microns (Ring-1) and 0.7 microns (Ring-0 inner most ring). Few concerns with the Si-wafer were (a) first, to keep the surface clean, and (b) second, the brittleness of the material. For this, the material was handled with care at all times. The Si-wafers were first washed with soap solution, followed by cleaning the surface with acetone. The final step involved washing this Si-wafer with methanol. These steps confirmed that the surface was clear of any polar and non-polar impurities. In between the steps, the Si-wafer was cleaned with deionized water in a sonicator. When not being used the Si-wafer was kept immersed in acetone.

2.4 Molding Process

The process of molding was carried out in absence of clean room environment to assess how robust and feasible the process is. The molding trial was carried out from the same piece of the molding material to eliminate variability caused by any difference in shape at different parts of the mold. After each molding trial, the tool surface needed to

be thoroughly cleaned. Various solvents were used in order to dissolve the polymer that might be adhering to the tool surface. In our trial runs, it was observed that the polymers, PS and PMMA that stuck to the mold surface were easily dissolved in toluene. After the PP parts were produced, the tool surface was cleaned by soaking it in chloroform and Methyl Ethyl Ketone (MEK) for a period 12 hours. Once sure the part is clean, the next polymer part was synthesized. Table 3 shows the procedure adopted for synthesizing various polymer parts. This mentions the molding temperature, time of molding and time of cooling for various polymers of this study. HDPE was the last to be molded on the surface as it showed high sticking and no appropriate solvent could dissolve it without being detrimental to the mold surface.

In order to form the mold the following steps were used. The polymer pellets were first weighed and then placed in an aluminum cylinder which was placed on the featured surface. For complete filling of features in the mold, it was required that the polymer had low viscosity. The molding was carried out at tool temperatures above the standard values given by plastic suppliers. The temperatures for molding of different polymers are given in Table 3.

Table 3 Temperature used for molding of the polymers.

Polymer	MoldingTemp (ºC)	Time of molding (mins)	Time of cooling/ demolding (mins)
HDPE	160	5	9
PP	200	5	9
PS	235	5	9
PMMA	250	5	9

The chamber was preheated to bring the surfaces and polymer in equilibrium. The temperature was the raised slowly at 1 ºC/minute until it reached the temperature at which a polymer melt forms, filled up and replicated the feature under ambient pressure conditions. Figure 8 shows the set-up used for this replication process. The only pressure applied in this molding process was due to the weight of the polymer melt. After the polymer cooled down at room temperature, the replicated part was removed from the tool surface by application of force. In this process, excess polymer pellets were used in the metal cylinder in order to facilitate this demolding of the replicated polymer from the tool surface. This also helped in achieving better replication since the weight of the polymer provided the applied pressure. The replicated part was then thoroughly cleaned with distilled water followed by drying in nitrogen atmosphere.

2.5 Characterization of Molded Part

(a) Dimensional analysis

The extent of dimensional stability of the part after feature replication was divided into 2 parts. For micro-feature analysis, scanning electron microscope (FE-SEM, S-4800, Hitachi, Japan) was used to calculate the differences in the dimensions of the tool and the part. For nano-feature analysis, both scanning electron microscopy (SEM) and atomic force microscopy (AFM) were used to calculate respectively the width and the depth of the features. SEM was not able to measure the depth in case of nano-featured surface due to the closed structure of the part synthesized. Percentage shrinkage in the dimensions of polymer parts was calculated from the SEM and AFM micrographs. The feature morphology and quality of replication was clearly evident from the SEM and AFM micrographs.

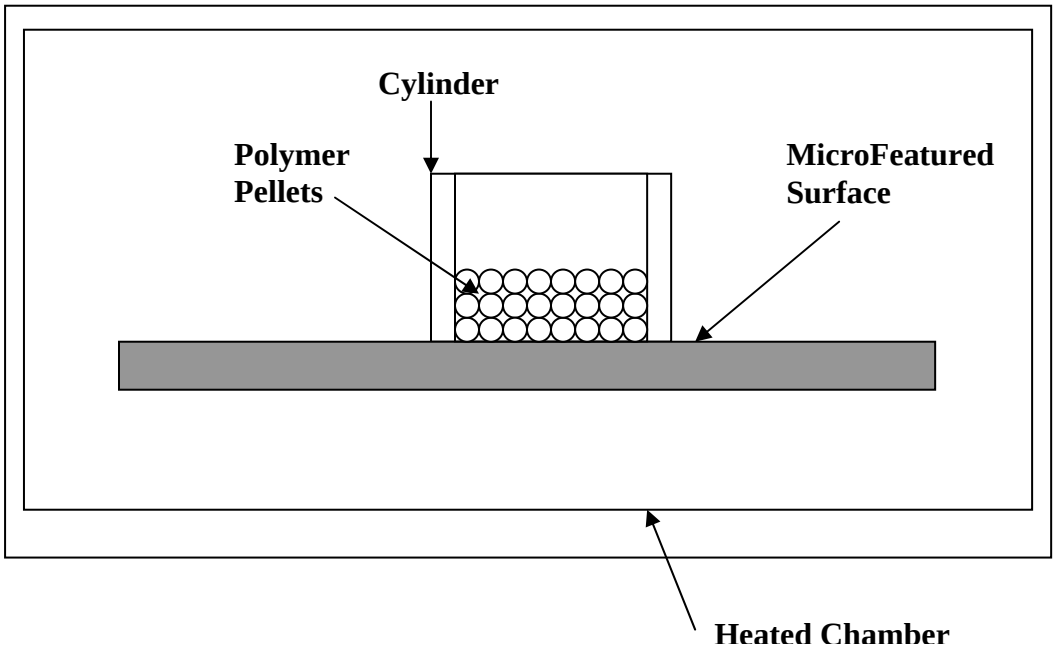

Figure 8 Set-up for the molding process performed.

(b) Feature replication

The feature replication quality was quantified by comparing the SEM micrographs and AFM data of the molded part with the tool material. For SEM, a field emission scanning microscope was used operated at 5kV. The SEM micrographs showed the qualitative differences in the feature replication. The surface topology of the mold and polymer parts was imaged using a Digital Instruments (Santa Barbra, CA) MULTIMODE™ AFM in contact mode with a Nanoscope IIIA SPM controller. The tip used was a Silicon Nitride contact tip supplied by Digital Instruments. The location of the surface to be scanned was marked and analyzed at the same place for the mold and the part. The histogram of each profile showed clearly the distribution of the depths of the mold surface. The change in aspect ratio (height/width) is also calculated from the AFM profiles. These AFM measurements performed the quantitative analysis of feature replication. The replication quality of the tooling feature was quantified by using depth ratio D.R.

$$DR. = \frac{d_p}{d_t} \qquad \text{…Equation (12)}$$

where, d_p is the depth of feature in the molded part and d_t is the depth of feature in the tool

(c) Roughness analysis

The AFM was also used to compare the surface roughness of the molded part with the mold surface. The roughness profiles of various areas in the polymer parts and the mold were observed and averaged to get the root mean square (RMS) value for the roughness. The RMS roughness value was calculated using the AFM image analysis

software. It was used to extract the profile measure dimension and roughness on and around the areas surrounding the features.

(d) Crystallinity Measurements

The measure of the extent of crystallinity in the molded parts formed was made by an x-ray diffractometer (XRD, XDS-2000, Scintag, Sunnyvale, CA, Cu K_{α}-tube). The polymer parts were placed in the quartz sample holder with the flat side oriented for the incoming x-rays to strike directly onto the surface. The scans were performed at 40 kV and 30 mA with a step size of 0.04° per minute. The XRD graphs of crystalline polymers showed characteristic sharp peaks, and the extent of crystallinity was measured by analyzing the area under the curve.

CHAPTER 3: RESULTS

3.1 Differential Scanning Calorimetry (DSC) Measurements

The DSC curves of all the four polymers have been given in Fig 9. Well defined peaks for HDPE and PP were shown in the DSC curves. These peaks correspond to the melting point T_m of the respective polymers. HDPE is crystalline in nature and PP is semi-crystalline and shows a sharp drop in heat conductivity while undergoing a phase transformation. The peaks are associated with the melting temperature (T_m) of the polymers. The T_m for HDPE was observed at 120.36ºC and for PP was observed at 163.72ºC. PS and PMMA showed smaller but distinct peaks representing the glass transition temperature T_g. Amorphous polymers gradually transform into a viscous state above their T_g. The indicated T_g for PMMA was between 80°C to 90°C and for PS was between 95°C and 105°C. The peaks on the DSC curves of PS and PMMA indicate some level of alignment in the polymers. These results were critical in determining the processing temperature for the polymer use. The temperatures used for study were well above the T_m and T_g of the polymers so that they are in a flow able melt state.

3.2 Contact Angle Measurement

(a) Theoretical surface energy tabulation

Four types of interactions contribute to the surface energy of a material. These constitute the polar and the dispersive components of the total surface energy. The intermolecular forces that contribute to the polar component of the surface energy are the permanent and induced dipoles and hydrogen bonding. The dispersion component of the surface energy is due to the instantaneous dipole moments.

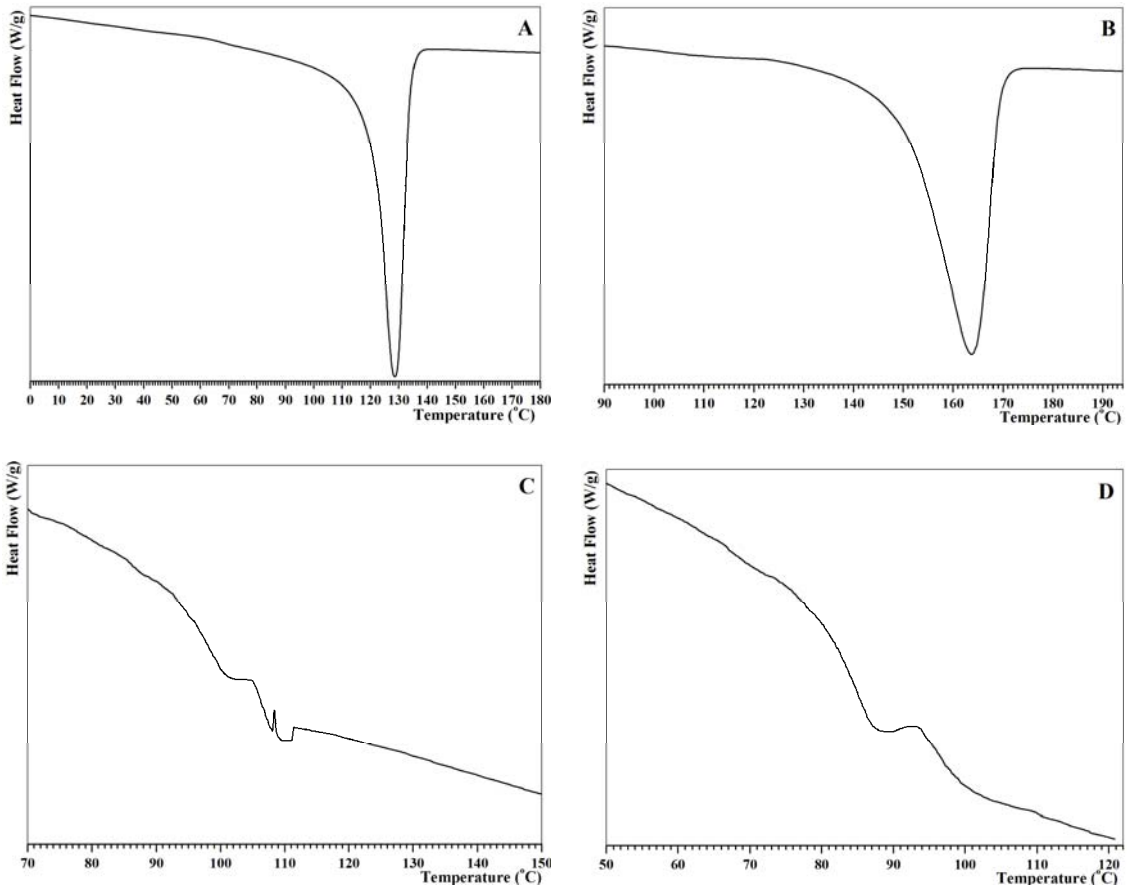

Figure 9 DSC curves for (a) HDPE, (b) PP, (c) PS, and (d) PMMA.

The surface energy of different solids was calculated by placing a drop of reference liquid on them. The estimation of surface energy was based on the following assumptions [70].

1. The total surface energy of solid and liquids are the sum of their dispersion and polar surface energy components.

2. The solid and liquid interact only by means of the dispersion and polar components.

3. The surface energy of the solid does not show considerable change with temperature.

A minimum of three reference liquids were used to accurately determine the surface energy of the molding surfaces under study. The reference liquids used were water, ethylene glycol and Glycerol. Their polar and dispersive components are given in Table 4. A similar method has been adopted by Kim and co workers [70] Barry, et al [16] and Opfermann and co workers [71] to measure the surface energy of various oxides and metal surfaces.

Table 4 Polar and Dispersive components of reference liquids

Reference Liquids	**Polar mN/m**	**Dispersive mN/m**	**Total mN/m**
Water	50.2	22.0	72.2
Ethylene Glycol	19.0	29.3	48.3
Glycerol	29.8	33.9	63.7

Atleast, 10 measurements of contact angle were taken on each surface by placing a drop of the reference liquid on them. The contact angle value θ was then substituted in the Owens-Wendt equation for calculating the surface energy.

$$1+\cos\theta = \frac{2\left(\gamma_s^d\right)^{1/2}\left(\gamma_{lv}^d\right)^{1/2}}{\left(\gamma_{lv}\right)} + \frac{2\left(\gamma_s^p\right)^{1/2}\left(\gamma_{lv}^p\right)^{1/2}}{\left(\gamma_{lv}\right)} \qquad \text{...Equation (13)}$$

Where, θ is the contact angle for the contact liquid; γ_s^d and γ_s^p are the dispersion and polar component of solid surface; and γ_{lv}^d, γ_{lv}^p and γ_{lv} are the dispersion, polar component and total surface energy of the contact liquid used.

Three contact liquids were used on the same surface, the values of γ_{lv}^d, γ_{lv}^p and γ_{lv} are found out from literature [72]. The dispersion and polar components of the solid surface energy can be obtained from equation 13 and solving three simultaneous equations formed by substituting the value of θ and the component values for respective reference liquids. The total surface energy of the solid surface is the sum of polar and dispersion components found out from the equation 14. The values obtained for the total surface energy of the solid is given in Table 5.

$$\gamma_s = \gamma_s^d + \gamma_s^p \qquad \text{...Equation 14}$$

Table 5 Surface energy of metals using reference liquids

Surface	Surface Energy (mN/m)
Stainless Steel	22.29
Tool Steel	25.48
Aluminum	81.00
Silicon	132.06

We observe that the surface energy calculated for the Aluminum and Silicon is relatively higher than the other two surfaces due to the oxide layer it forms readily on its surface during exposure. Zisman and co-workers reported the critical surface tensions of metals and metal oxides in the contact with liquids are about 47 to 36 mN/m [25]. These values are smaller than those we have measured for the oxide surfaces. However, we note that the method employed by Zisman and co-workers estimates a critical surface tension

(γc) which is always smaller than the surface energy, because γc is obtained by neglecting the interfacial tension between the solid and liquid and the equilibrium spreading pressure. The values calculated are not absolute values of surface energy but a relative measure of the surface properties of the metals for comparison purposes. The deviations observed could be due to impurities present on the surface.

It is well known that the surface energy of polymer decrease with the increase in melt temperature. The theoretical surface energy of the polymer melts was tabulated from the data given in the Polymer Handbook [73], knowing the rate of change of surface energy with temperature the surface energy of the melt at the temperature of concern were calculated as shown in Table 6. Polymers rate of spreading would be fastest when all the three surface tension factors favoring the spreading should be met. Theoretically, the surface having minimum interfacial tension with respect to the polymer melt coupled with high surface energy of solid and low surface tension of liquid are considered positive factors for the polymer to spread appreciably.

Table 6 Surface energies of all polymers of this study [73] .

Polymer	**Temperature**	**Surface Energy(mN/m)**
HDPE	145	29.68
	160	28.80
PP	185	20.14
	200	19.30
PS	220	26.00
	235	24.90
PMMA	240	24.30
	255	23.35

(b) Experimental rate of spreading measurements

The experimental rate of spreading was determined by plotting the change in contact angle versus the time. These time profiles were used to determine the rate of spreading of each polymer on a particular surface. It was taken into consideration that the initial contact angle was largely dependent on the original particle shape as well as the melting properties of the polymer such as the thermal conductivity, heat capacity and zero shear viscosity. Initial experimentation on the polymer also showed that the time of incubation of polymers to melt was around 9 minutes. Thus the contact angle measurement was started after an interval of 9 minutes of setting the temperatures as given in Table 2. Only the first two or three points can be considered as the artifacts of the initial attributes of the polymer bead on the surface. The influence of time on the evolution of the contact angle gives us a fair idea on the wettability of polymer on contact surfaces. The experimental trials were carried out in triplicate to confirm the values of spreading rate. The trend for the four polymers on different surfaces at the lower temperatures (Set 1) can be seen in Fig 10.

The slopes were tabulated from each of the graphs by fitting a linear regression line on each curve and then tabulating its slope by the equation of the line. A higher slope of the curve indicates a faster spreading rate on a given surface. The slopes have been tabulated in the Table 7.

Table 7 Magnitude of rate of spreading at low temperatures

	Al	**SS**	**TS**	**Si**
HDPE	-0.0554	-0.0475	-0.0290	-3.0494
PP	-0.0634	-0.0805	-0.0917	-3.2146
PS	-0.1250	-0.0582	-0.0442	-6.2857
PMMA	-0.0716	-0.1273	-0.0693	-3.6462

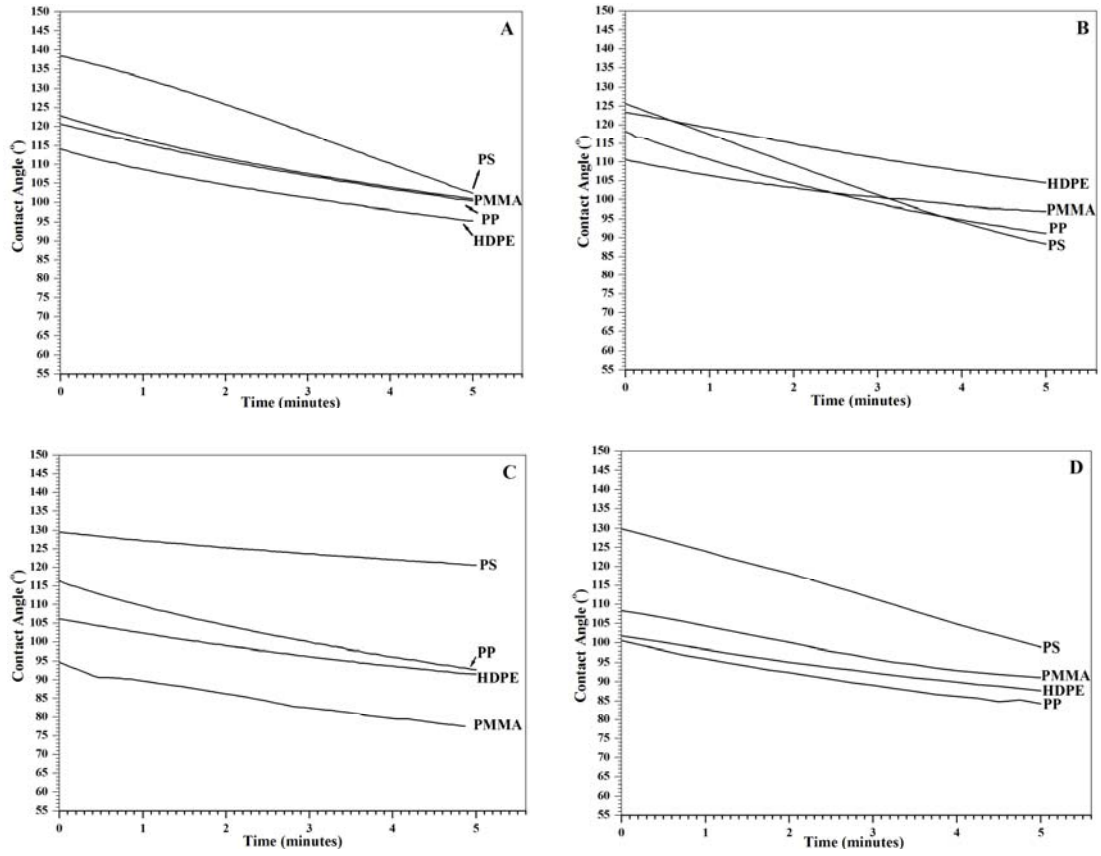

Figure 10 Contact angle measurements performed at low temperatures to determine rate of spreading of HDPE, PP, PS and PMMA on (a) Aluminum, (b) Stainless Steel, (c) Tool Steel, and (d) Si-wafer

It was observed that for Aluminum and Silicon surfaces PS and PMMA showed the highest spreading rate at lower set of temperature. This was followed by PP and finally HDPE. In Tool Steel and Stainless Steel there was an increment in the spreading rate for PP. HDPE consistently showed the lowest value of spreading rate for all the surfaces. However PMMA and PS consistently showed the fastest spreading rate for almost all the surfaces. It was observed that after an initial interval of time PMMA exhibited spreading with a drop having a shape of a cap with foot as shown in Fig 11. Thus, the goniometer in the instrument imaged a lower contact angle. This shape was also exhibited by PS on the surface of Aluminum and Silicon. On the contrary PP and HDPE spread on the surfaces with a spherical shape as shown in Fig 12. Overall, the magnitude of slopes did not show high variation and the spreading rate on surfaces was almost similar for polymers except for on aluminum and silicon. After this the rate of spreading of polymers was observed on the same set of surfaces with a temperature increment of 15°C, that is, temperature Set 2. The spreading behaviors can be seen in Fig 13.

It was observed that with the rise in temperature the magnitude of slopes increased drastically as seen in Table 8. The incubation period of the formation of liquid drop decreased and the change in the contact angle values became very rapid. The highest rate of spreading was again observed for Silicon surface but there was not much change in the magnitude of slopes with increase in temperature. For the other 3 surfaces the rate of spreading was similar. The polymers followed a similar trend of spreading on silicon (Si) and aluminum (Al). There was no change in spreading trend at high temperatures on these 2 surfaces. HDPE showed slowest spreading rates on all surfaces even with the rise in temperature. However PP again showed faster spreading rates on tool steel and

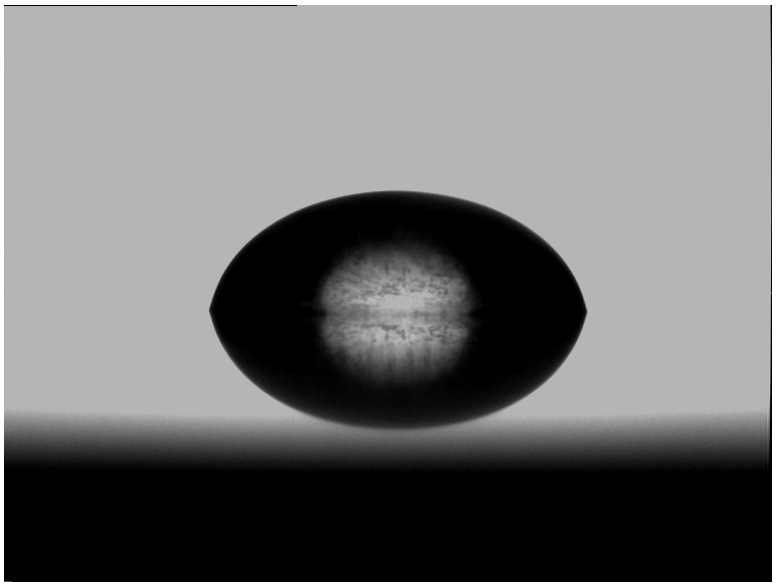

Figure 11 Spreading of PP drop in “Spherical shape” on Al surface.

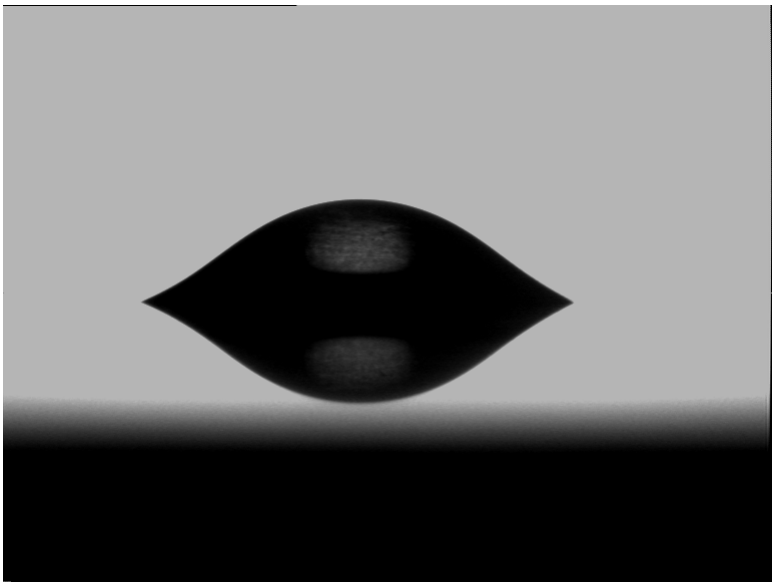

Figure 12 Spreading of PS in “Cap with foot shape” on Al surface.

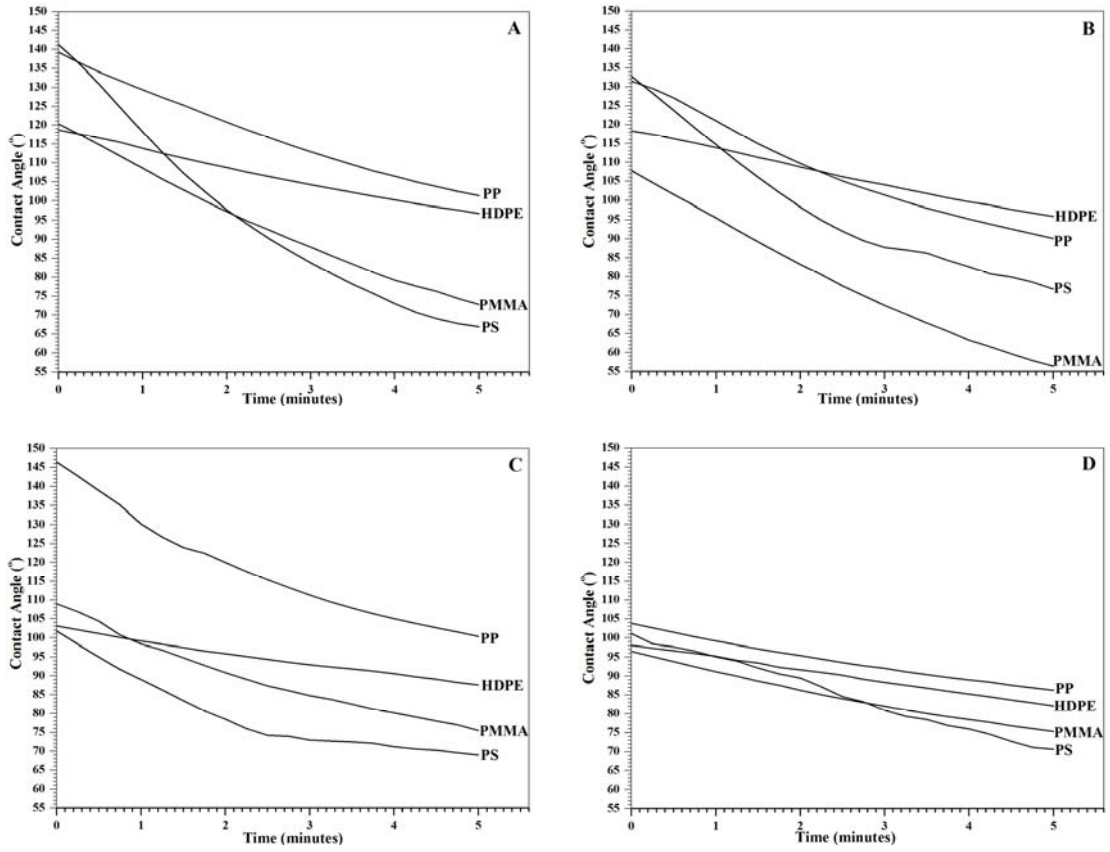

Figure 13 Contact angle measurements performed at high temperatures to determine rate of spreading of HDPE, PP, PS and PMMA on (a) Aluminum, (b) Stainless Steel, (c) Tool Steel, and (d) Si-wafer.

stainless steel. Thus an inconsistency in the normal trend was observed on tool steel and stainless steel surfaces with PP. Except for HDPE all the polymers showed a cap with foot shape while spreading on the surfaces.

Table 8 Magnitude of rate of spreading at high temperatures

Polymer	**Al**	**SS**	**TS**	**Si**
HDPE	-1.1148	-1.1527	-0.7484	-3.2515
PP	-1.9027	-2.7240	-2.0148	-4.2566
PS	-3.6060	-2.1194	-1.6178	-6.3100
PMMA	-2.4008	-2.6186	-0.7484	-3.4561

As seen from the experimental values the different polymers were ranked according to the extent of spreading on a particular surface, the best being the one that has the highest slope or spreads the fastest. The ranks are as in Fig 14 for temperature set 1 and in Fig 15 for temperature set 2. It can be correlated that the polymer spreading fastest on a particular surface will show best wettability and thus show good feature replication in a molding process. It can be clearly seen that PMMA and PS should give the best feature replication on almost all the surfaces, as they show the fastest spreading rate. HDPE should show the lowest extent of feature replication. PP will show better feature replication with Steel surfaces than for Silicon and Aluminum. PS and PMMA gave almost similar spreading behaviors. This data can be useful in prediction of polymer and mold/tooling surfaces that can be used to attain maximum feature replication the micro injection molding process.

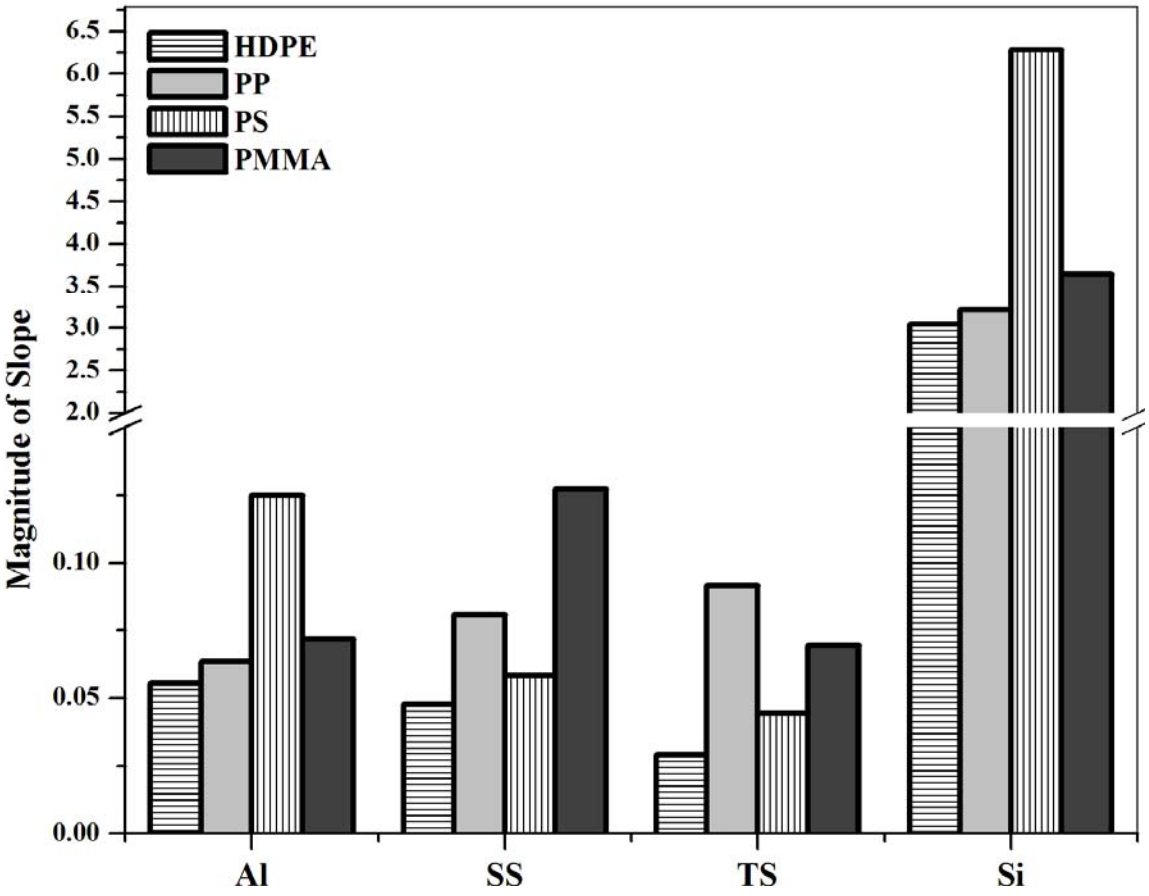

Figure 14 Graph showing the comparative ranks of different polymers on different surfaces of this study at low temperatures

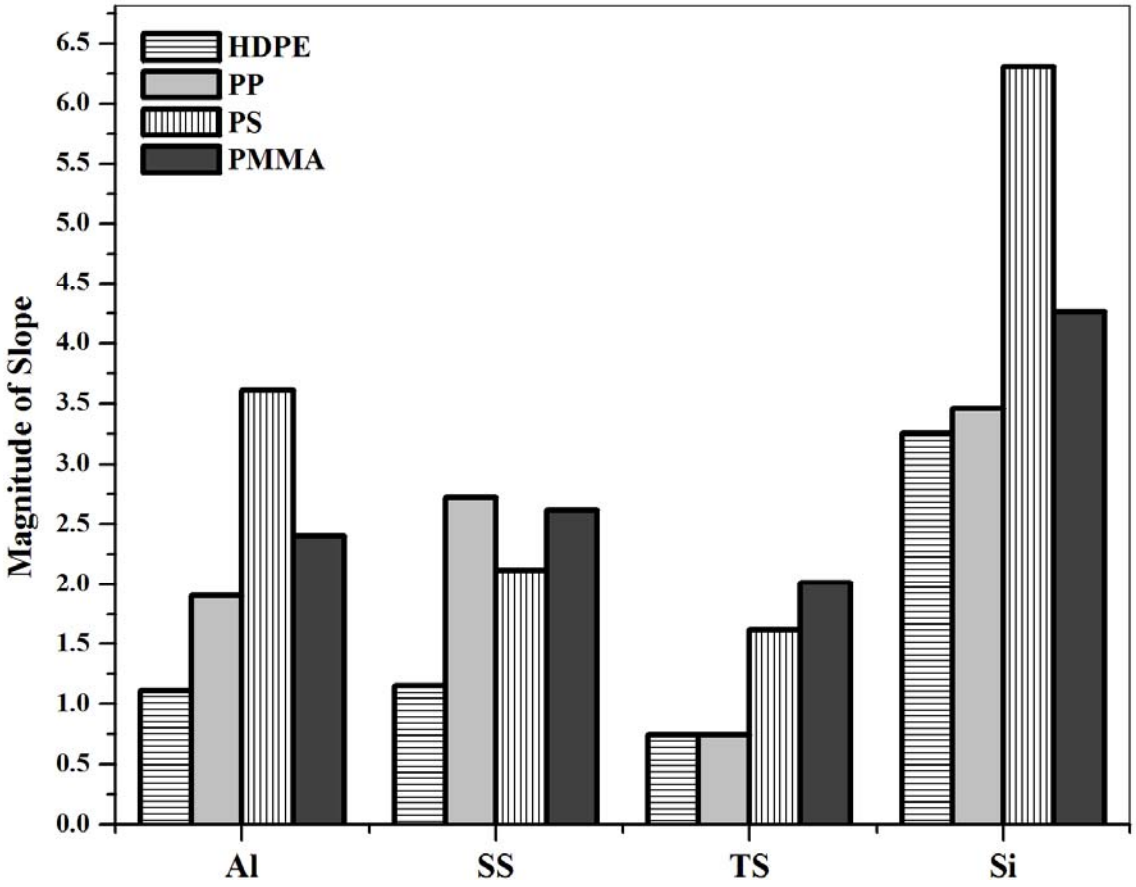

Figure 15 Graph showing the comparative ranks of different polymers on different surfaces of this study at high temperatures

3.3 Viscosity

The rate of change of viscosity with change in shear rate was plotted and all polymers behaved as power law fluids showing thinning behavior. The plot of the shear rate vs. the melt viscosity is given in Fig 15 . The data was obtained for a shear rate from 10 sec^{-1} to 10,000 sec^{-1} and for temperature data set 1 and set 2. Most of the polymers exhibit a Newtonian plateau at low shear rates, a transition region after that, and then a region where the polymer behaved as a power law fluid. At rates greater than 500 sec^{-1} all the polymers became less viscous and started showing some extent of shear thinning. Shear-thinning fluids have a lower apparent viscosity at higher shear rates. It is generally supposed that the large molecular chains tumble at random and affect large volumes of fluid under low shear, but that they gradually align themselves in the direction of increasing shear and produce less resistance. All four polymers in the study showed shear thinning behavior at high shear rates. The power law index, n, has been used to quantify the shear sensitivity of the melt viscosity. As the power law index increases the polymer becomes more sensitive to the increase in shear rate and thus shows more shear thinning. The data of viscosity and shear rate was plotted on a log-log scale and a power law regression line was fitted to it for the shear rates above 500 sec^{-1}. The rate of shear thinning index was tabulated from the slope of the plot for polymers at different temperature and shown in Table 9. The power law index was calculated from equation 3. With increase in temperature PMMA shows maximum increase in the shear thinning. HDPE shows the least variation in shear thinning with temperature due to its long chained structure.

Table 9 Power law index for polymers of this study at the used temperatures

Polymer	Temperature	n
HDPE	145	0.47
	160	0.51
PP	185	0.34
	200	0.36
PS	220	0.26
	235	0.34
PMMA	240	0.32
	255	0.52

It can be seen that from Fig 16 that PMMA was the least viscous at 255 °C and PS was the most viscous at 220 °C at low shear rates. The magnitude of viscosity at shears below 10 sec^{-1} can be evaluated by extrapolating the graph from the Newtonian plateau. At temperature Set 1 the viscosity at very low shear rate is the lowest for PP followed by HDPE, then PMMA. PS has the highest viscosity at temperature Set 1. At higher temperatures (that is, Set 2) and low shear rate, the trend was different from the previously observed data. PMMA showed minimum viscosity, followed by PP and then HDPE. PS again showed the maximum viscosity at high temperatures. The viscosity effects can be used to explain the variations that were shown in the rate of spreading data. The lower viscosity the more likely will be the penetration of the polymer fluid in the features thereby making it potentially better for feature replication in micro-injection molding.

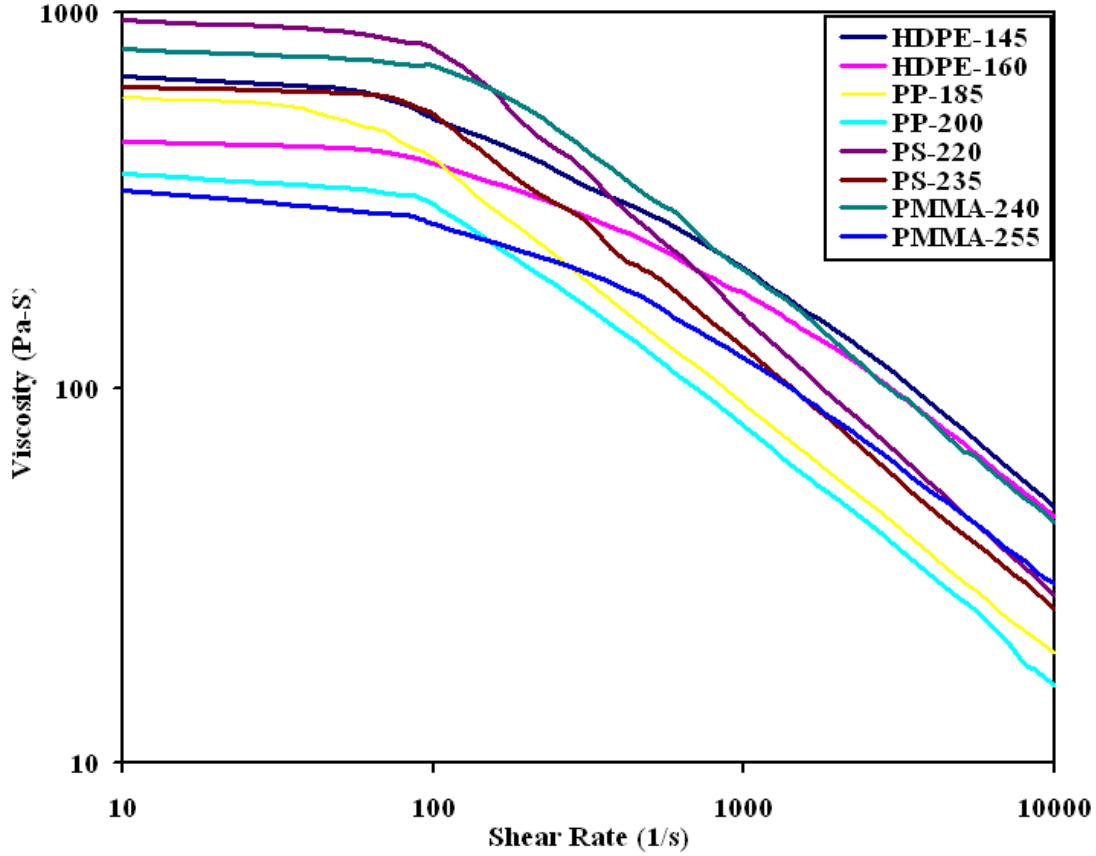

Figure 16 Viscosity-shear rate relationship for the polymers of this study at temperature set 1 and set 2.

3.4 SEM Study

(a) Micro-featured surfaces

The SEM micrographs of the replicated parts were taken from top and cross-section in order to analyze their dimensional stability. The dimensional measurement was performed by the Quartz PCI software, after the micrograph was taken. Due to the variability in the dimensions across the feature statistical sample size was taken as 50, that is, 50 different observations were measured for both height and elevations. Thus, for both set of dimensions, the mean and their respective standard deviation are reported. Similar measurements were performed on the stainless steel mold part. Afterward, values of part and mold were compared, thereby, providing a scenario of changes in dimensions. This helped in comparing the dimensional stability of the parts synthesized using different polymers. Figure 17 shows the SEM micrograph wire EDM micro-grooved of stainless steel part. This part shows a wide grooved region and a thin elevated region. From the micrograph, the minute craters/depressions formed on the surface due to wire EDM process are also clearly visible. After the part was formed, the SEM micrograph showed a wide elevated region and a thin grooved region. From the micrographs, it is seen that the craters/depressions present on SS surface have been replicated by the polymer parts, indicating a good replication quality. This suggests that the polymer flows easily on the surface when molding was performed at elevated temperatures and ambient pressures. All the four polymers of this study showed the same response. Also observed were differences in dimensions and surface inconsistencies between part and mold which indicated the quality of the part produced. These defects can be divided into two, first is the polymer tear off that is related to the polymer adhesion to surface and second is

shrinkage that is related to the crystallinity and basic polymer properties. In case of HDPE (Fig 18a), maximum polymer tear off due to demolding. It can be observed that the due to the shear force experienced by the polymer during ejection, a portion of the part was sheared in between the grooved and elevated section, throughout the section. This trend is followed by PP (Fig 18b), which had lesser extent of this tear. This effect was not observed in PS and PMMA as can be seen in Fig 18c and 18d respectively due to their ductile nature.

Another defect was shrinkage which indicated low dimensional stability for all the polymers. This shrinkage can be computed by calculating the change in dimension observed in the (a) width of grooved and elevated regions, and (b) height of the elevated portion. The SEM micrographs presented in Fig 18 were sufficient to calculate the shrinkage as mentioned in part (a), that is, of width and elevated regions. The shrinkages observed in the width are presented as a graph in Figs. 19 and 20. The graph (Fig 19) shows the comparison of width of the grooves in the polymer parts with that of the mold. The graphs show that a considerable amount of decrease in the widths was observed. The minimum change in the mean value of dimensions was observed for PS whereas the maximum change was observed for HDPE. Now considering the length of error bars, dimensional change for all of the polymers overlaps. The graph in Fig 20 shows the comparison of the width of the elevations in the polymer parts with that of the stainless steel mold. This graph shows a high magnitude of the shrinkage between the polymers. Very large decrease in dimensions was observed for HDPE. Generally more crystalline polymers were showing higher shrinkage. The original dimension of the stainless steel tool is 355 μm whereas that of HDPE part had an average width of 325 μm representing

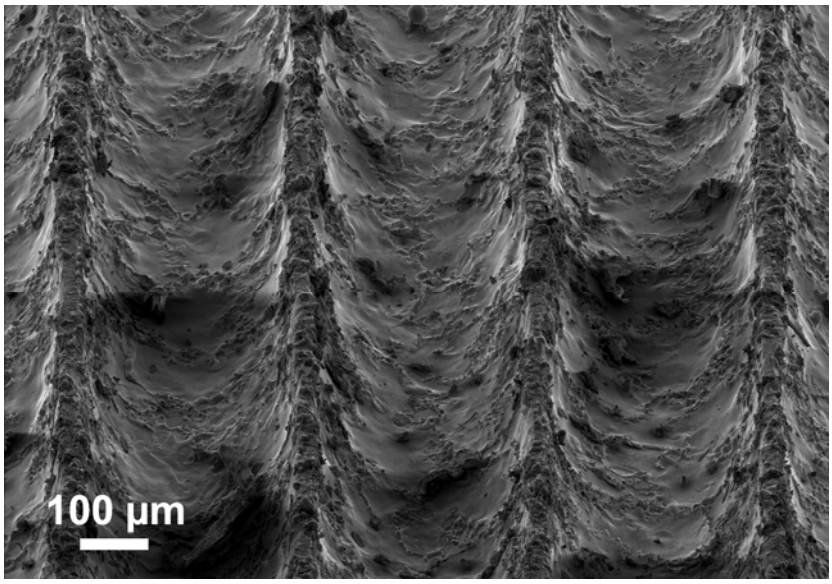

Figure 17 SEM micrographs showing top-view of stainless steel mold

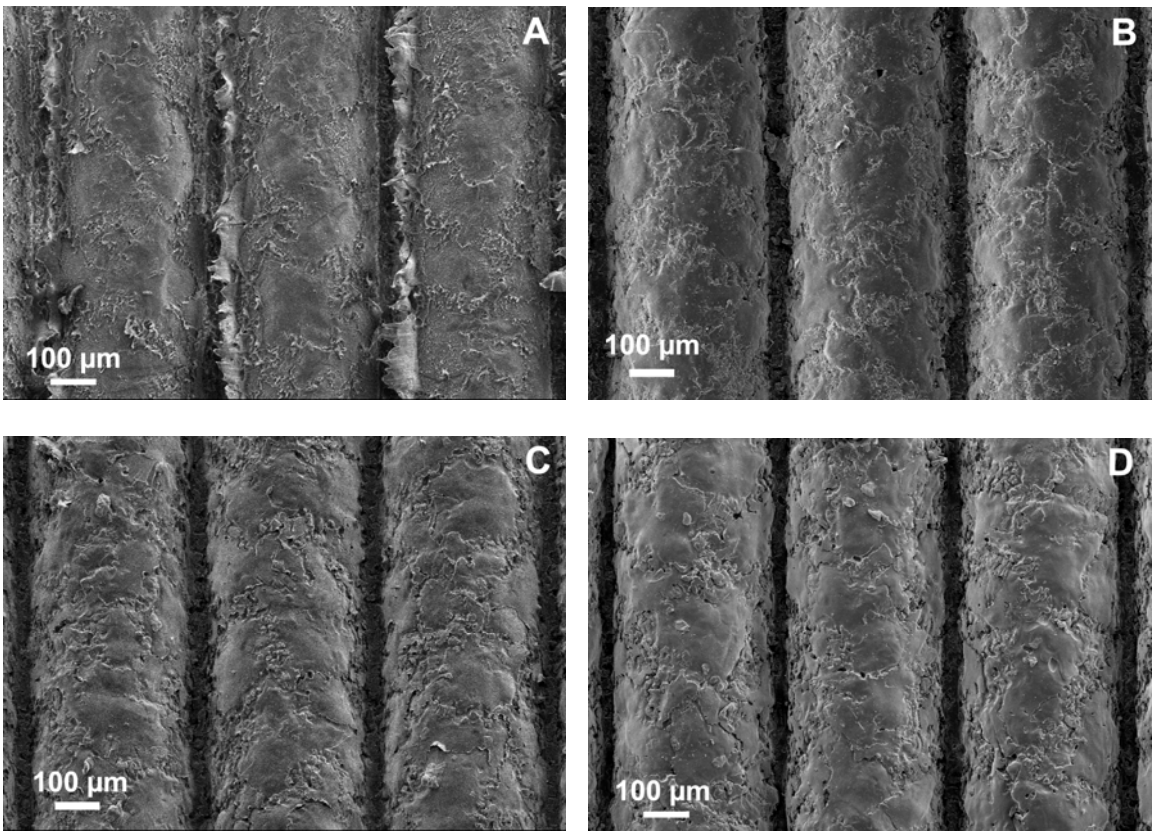

Figure 18 SEM micrographs showing top view of (a) HDPE; (b) PP; (c) PS; and (d) PMMA parts.

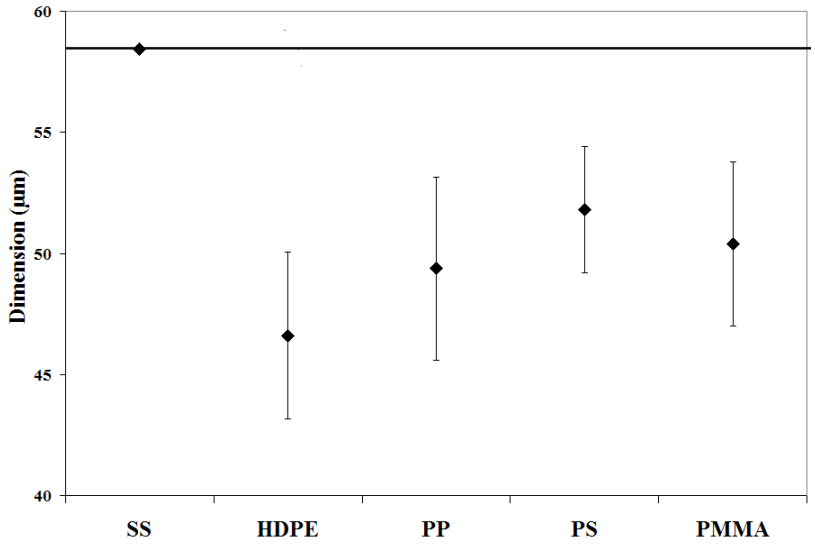

Figure 19 Dimensional changes observed in the widths of grooved surface of HDPE, PP, PS and PMMA parts in comparison to SS mold

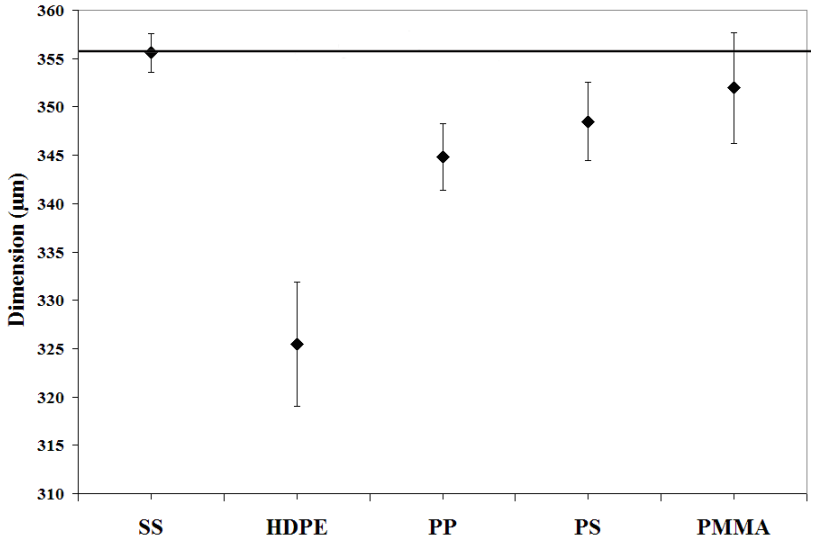

Figure 20 Dimensional changes observed in the widths of elevated surface of HDPE, PP, PS and PMMA parts in comparison to SS mold

shrinkage of around 10 %. In case of other polymers of this study, minimum of 2% dimensional change was observed for PMMA. In this case also, on consideration of the error bars, the dimensions of PP, PS and PMMA were overlapping.

The height of the elevated part in the mold was 177 μm, which was provided by the manufacturer of the mold. This was kept as the standard for comparison with the heights of the polymer parts. In order to determine the heights of the elevations in the parts, they were sliced enabling a clear view of the cross section. The SEM micrographs of the isometric view for all the cross-sections are shown in Fig 21. The tear off that was observed in top-view micrographs of HDPE and PP, was also seen here. The SEM micrographs show well defined trenches and walls in the feature. There was considerable decrease in the dimensions of the height for all polymers. The shrinkage was again the maximum in HDPE, with the value dropping to 131 μm. The minimum shrinkage was observed in case of PS. Another interesting effect observed in this case was that the shrinkage in height of the elevated region was very consistent, that is, the length of the error bars was small as shown in Fig 22.

These results show that the shrinkage was observed more in vertical direction than in horizontal. These results are corroborated by the naked eye examination, which show that on cooling the height of the part contracted more than the width of the part. This happened due to the preferential alignment of the polymer during flow in the cavity. Also, the percent shrinkage observed in all the polymer molds with respect to stainless steel mold is calculated. This data is shown in Table 10. The data confirms that the maximum shrinkage was observed in case of height of the elevations in comparison with the width of the elevations.

Table 10 Percentage shrinkage in the dimensions of the micro-featured parts

	Depression	**Elevation**	
	Width	**Width**	**Height**
HDPE	13.74%	8.48%	25.61%
PP	11.31%	1.02%	23.92%
PS	15.48%	2.47%	20.43%
PMMA	11.66%	2.00 %	22.22%

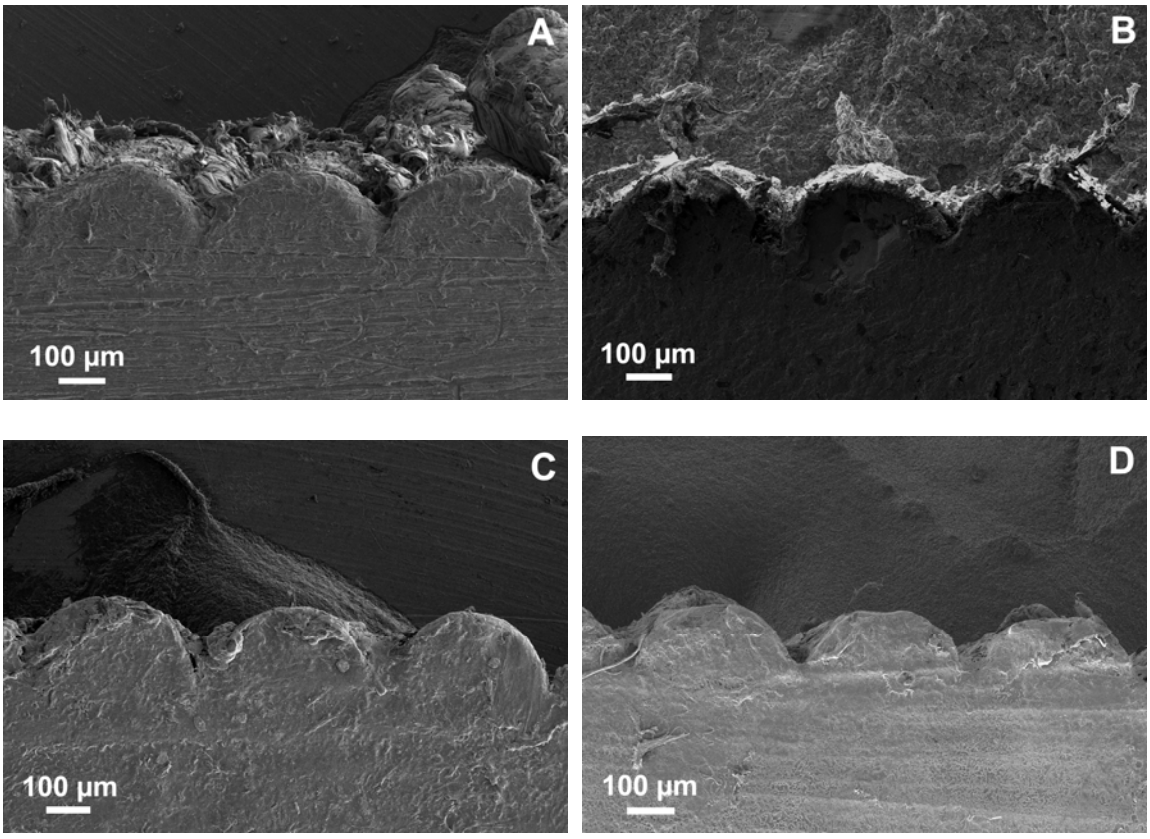

Figure 21 SEM micrographs showing cross-sectional view of (a) HDPE; (b) PP; (c) PS; and (d) PMMA parts.

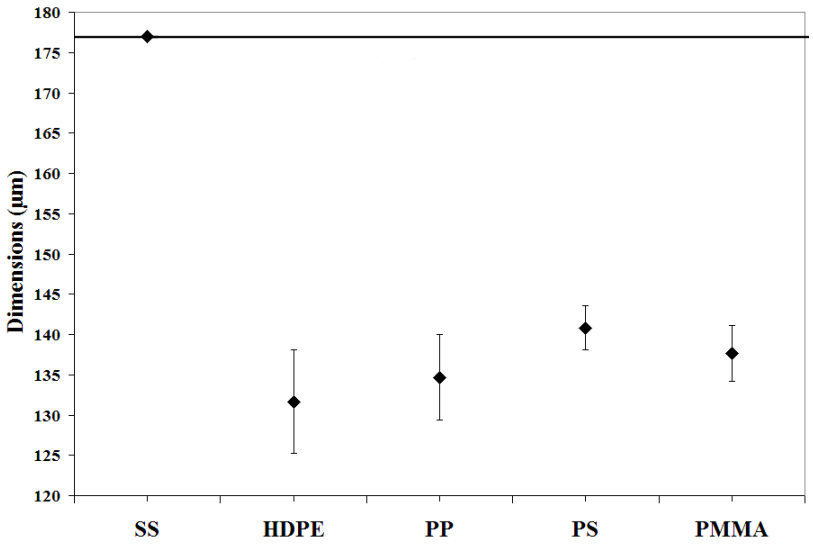

Figure 22 Dimensional changes observed in the heights of elevated surface of HDPE, PP, PS and PMMA parts in comparison to SS mold

(b) Nano-featured surfaces

As shown in section 2 of this study, the nano-features made by the DRIE process had 5 concentric rings of varying thickness. The depth of each ring was around 600 nm. In this way a varying aspect ratio is achieved in the same feature, thereby simultaneously examining the replication quality of different polymer with varying aspect ratio was made possible. The SEM micrographs of the nano-featured Si-wafer are shown in Fig 23 The surface had an overall uniform dimensions and an equivalent section width throughout the whole wafer.

The SEM micrographs of the molded polymers parts are shown in Fig 24. The SEM micrographs clearly show that the features were well replicated in all the four polymers. Even the smallest inner ring has a well defined structure. But due to the sticking nature and ductility of HDPE and PP pull-offs are seen on sides of the elevations. This is because of the application force caused while de-molding which led to tearing off of the polymer from one side. The pull off area is exaggerated in the rings having smaller thickness. Although the clarity and sharpness of features was appreciable the surface was unclean because polymer parts picked up dust particles very rapidly. It is observed that the outer ring had very well defined feature definition as compared to the inner rings. A dimensional analysis was performed on the polymer parts and the Si-wafer. This was similar to the one performed previously in case of micro-features. In the case of micro-features, measure of both, width and height of the features were performed by SEM. In nano-features, SEM was not used to measure the height; instead, AFM measurements were performed. The width of each ring is calculated and presented in Table 11. More shrinkage in the widths of all parts was observed as the ring thickness decreases. Of all

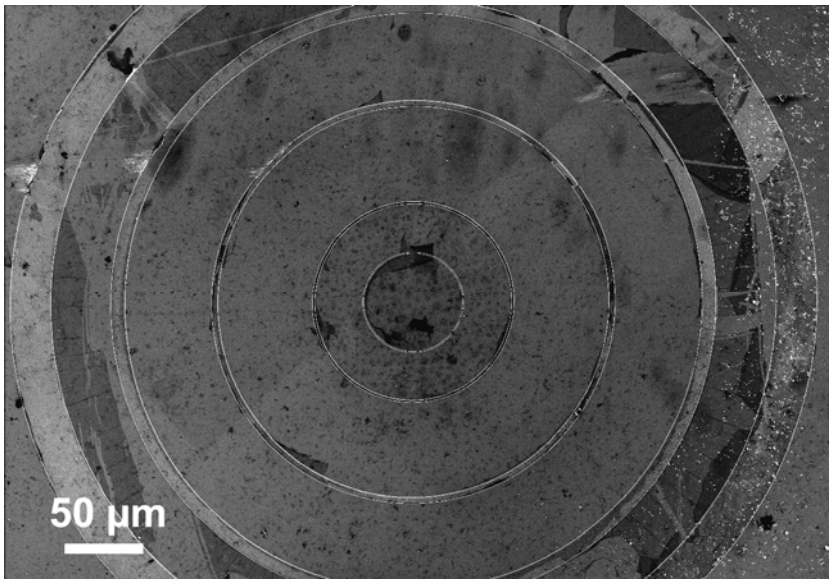

Figure 23 SEM micrograph showing the nano-feature that consists of 5 concentric rings etched on the Si-wafer

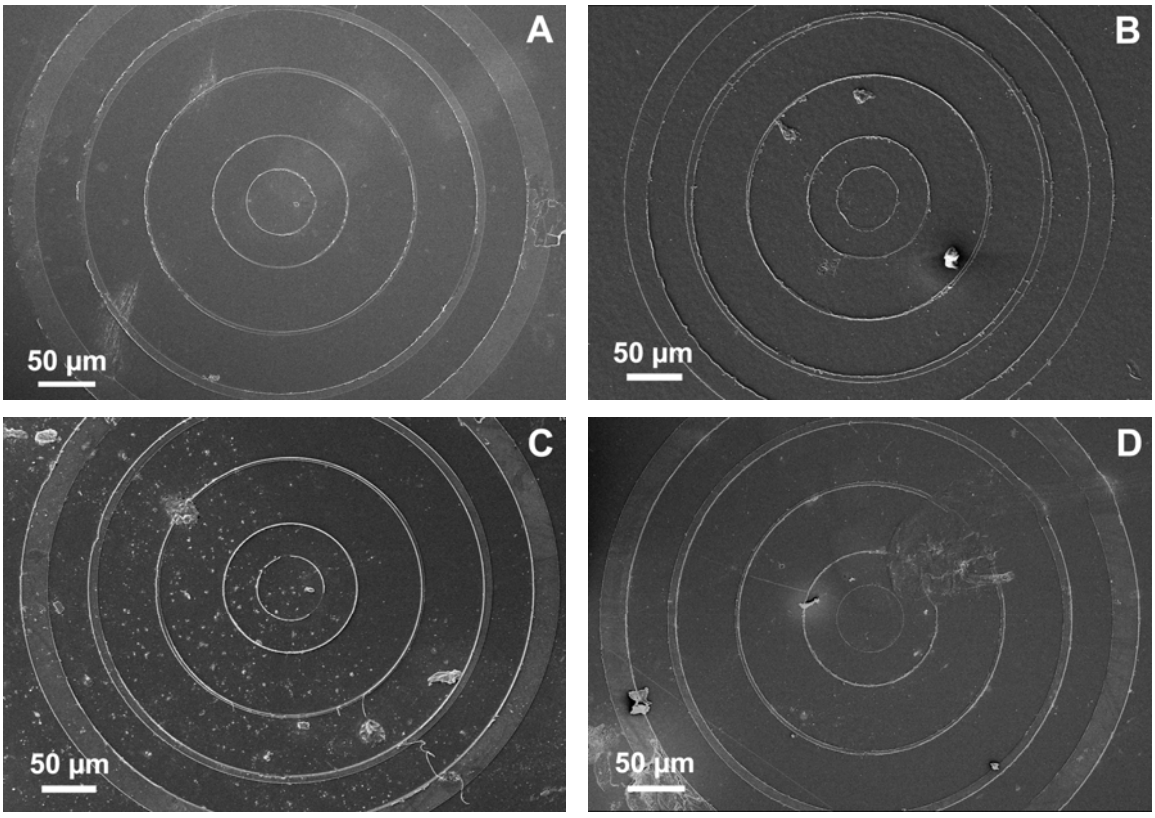

Figure 24 SEM micrographs showing top view of nano-featured (a) HDPE; (b) PP; (c) PS; and (d) PMMA parts.

the polymers, HDPE showed the minimum dimensional stability caused by shrinkage effects irrespective of the ring thickness. On the other hand, PS and PMMA performed better and much less shrinkage was observed in these 2 polymer parts. The graph presented in Fig 25 shows the percent shrinkage in various polymer parts at different ring thicknesses.

Table 11 Variation in dimension of polymer parts in comparison with Si-wafer at different ring thicknesses

	Si	**HDPE**	**PP**	**PMMA**	**PS**
Ring 0	0.670	0.450	0.47	0.52	0.51
Ring 1	1.223	0.730	1.12	1.03	1.15
Ring 2	3.650	3.264	3.380	3.44	3.49
Ring 3	7.958	7.762	7.940	7.78	7.41
Ring 4	24.05	23.16	23.10	23.22	23.33

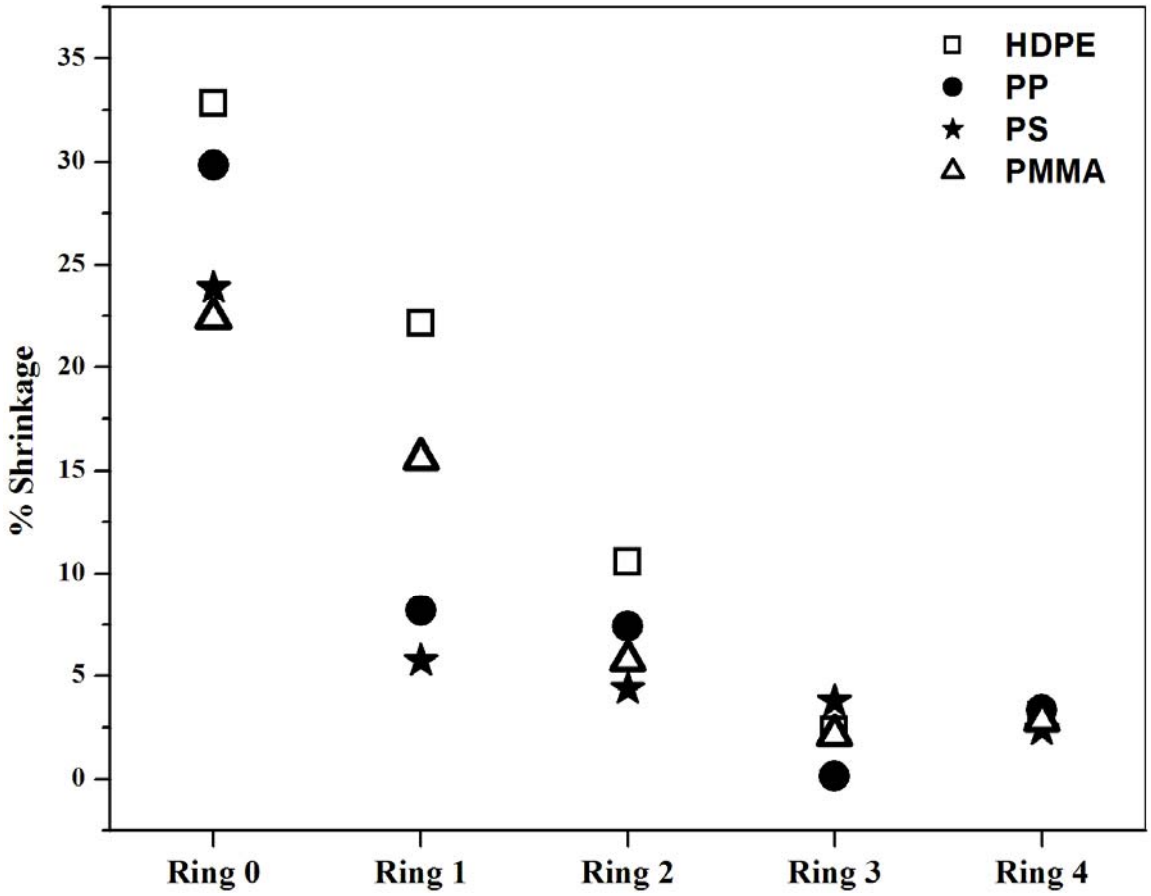

Figure 25 Percent shrinkage in the width of different rings of nano-featured polymer parts

3.5 AFM Analysis

(a) Micro-featured parts

The wire EDM process usually leaves the surface of the stainless steel with small craters and holes which were visually evident on the surface. These small micro features caused by sparking along with the general irregularities in the surface attributed to the roughness of the stainless steel mold. For the extent of feature replication it was observed how well the polymer penetrated into surface roughness features. As shown in Fig 27 the AFM topographs were used to estimate the roughness of the different surfaces. The scan was made over 10 microns x 10 microns square sections on the steel surface. Similarly roughness was calculated for the polymer surface at different places over the same area and an average estimate of roughness was calculated. As seen in Fig 26 the polymers showed lower roughness values than the stainless steel mold. The possible reason could be non replication of the micro holes present on the steel surface by most of the polymers. Due to irregularity of the surface the roughness caused due to sticking of polymer was also very high for HDPE and PP. The highest surface roughness was showed by HDPE with an RMS value of 128 nm. PMMA had the lowest surface roughness at 55 nm.

(b) Nano-featured parts

Dimensional analysis

Figure 28 illustrates how the depth and the width values were obtained for the polymer features from the AFM scans of cross sections. The topographies investigated were primarily trenches and projections shown by the AFM scans. The intensity of the

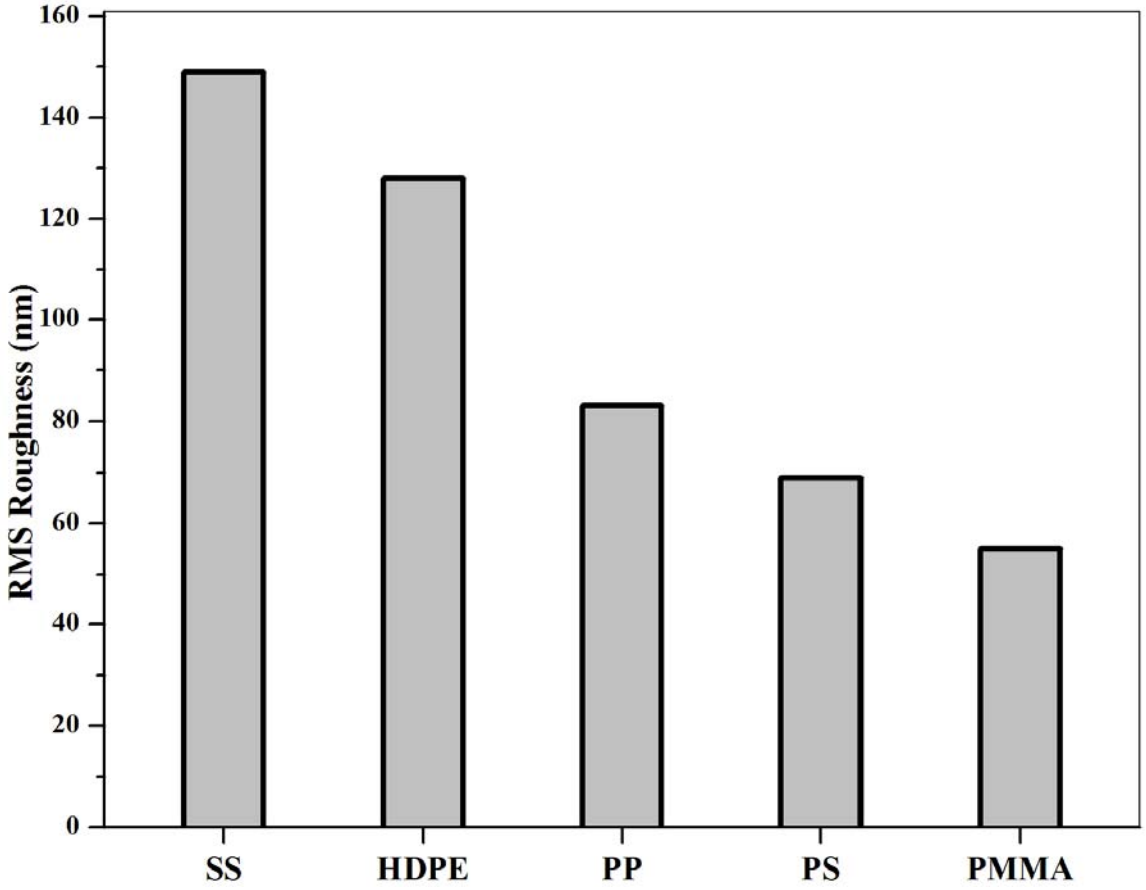

Figure 26 Magnitude of surface roughness of the surface of steel in comparison with the 4 different polymers.

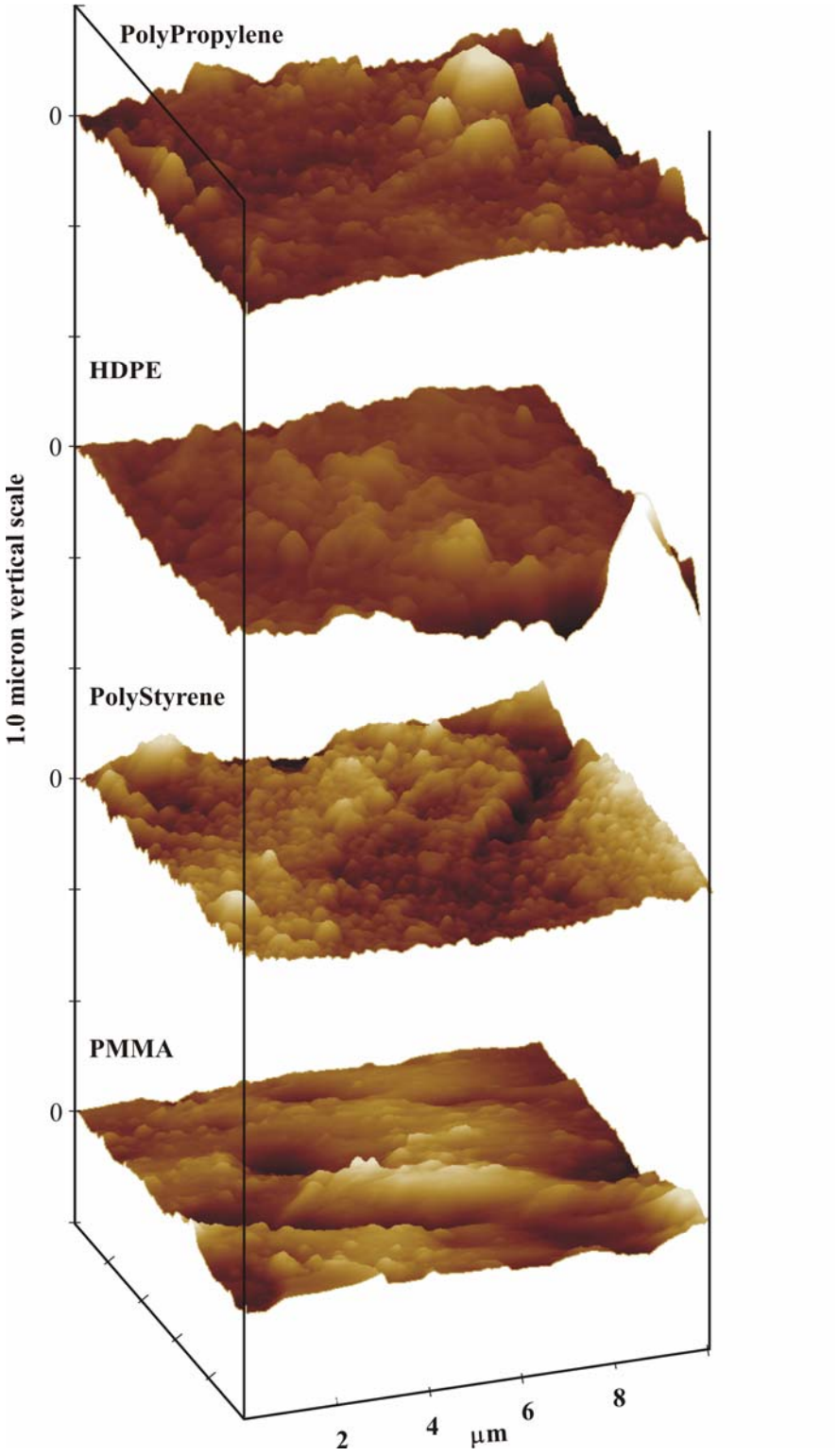

Figure 27 AFM topographs showing comparative roughness of the 4 polymers of a 10 micron x 10 micron area.

AFM signal was plotted as the function of depth. Since the average distance between the top of the plateau and the bottom of the trench was defined as the depth, the gap between the mean values for the bottom from the histogram were used to calculate the depth of the cross sections. The projections in the polymer parts had very steep walls but showed rounding off at the top indicating a loss in the feature resolution during molding of the part with the increase in aspect ratio as shown in Fig 29 and Fig 32.

Fig 30a & 30b shows the three dimensional view of the silicon tooling before molding and the molded PMMA part for the same feature. The silicon tooling showed an average trench depth of about 450 nm and aspect (depth/width) ratios ranging from 0.5 to 0.01. As indicated in Fig 32 the walls of polymer projections molded were relatively vertical and there were sharp corners at the bottom of the projections for all the 5 rings of varying aspect ratios. But the projections showed some rounding off and tear at the edges at the top indicating loss in feature quality as shown in schematic diagram in Fig 29. The AFM image in Fig 29 illustrates incomplete feature replication in the molded part. The polymer melt has not completely filled the features in the grooved Si part, resulting in a part surface contour that does not match the surface contour of the mold.

The extent to which polymer effectively filled the surface can be measured by comparing the height of the feature in the molded polymer part to the depth of trench in the Si mold. Since after the molding the trenches become projections in the molded parts, the notation “top’ and bottom” in tables refer to the projection and trenches, respectively, in the molded parts for convenient comparison as shown in Fig 31. Fig 32 clearly shows that the depth ratio given by Equation 12 was considerably low for the rings having high aspect ratio of 0.5 but became similar after the aspect ratio decreased below 0.3.

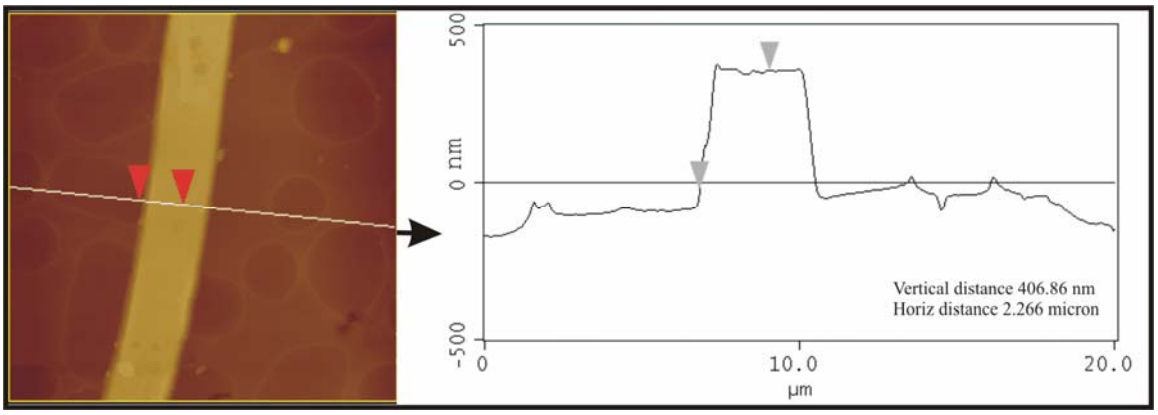

Figure 28 Section analysis of a PMMA ring for height and width measurement

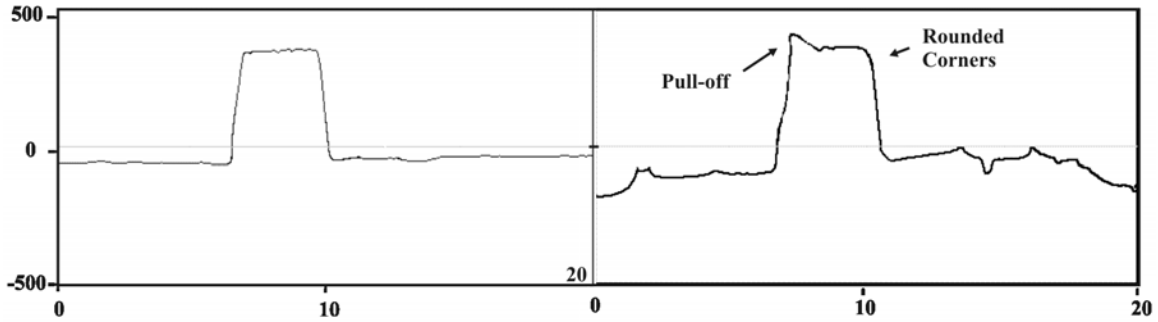

(a) (b)

Figure 29 (a) AFM image of good feature replication in a PMMA part. (b) Rounded off corners and pull off shown in HDPE parts having high aspect ratio.

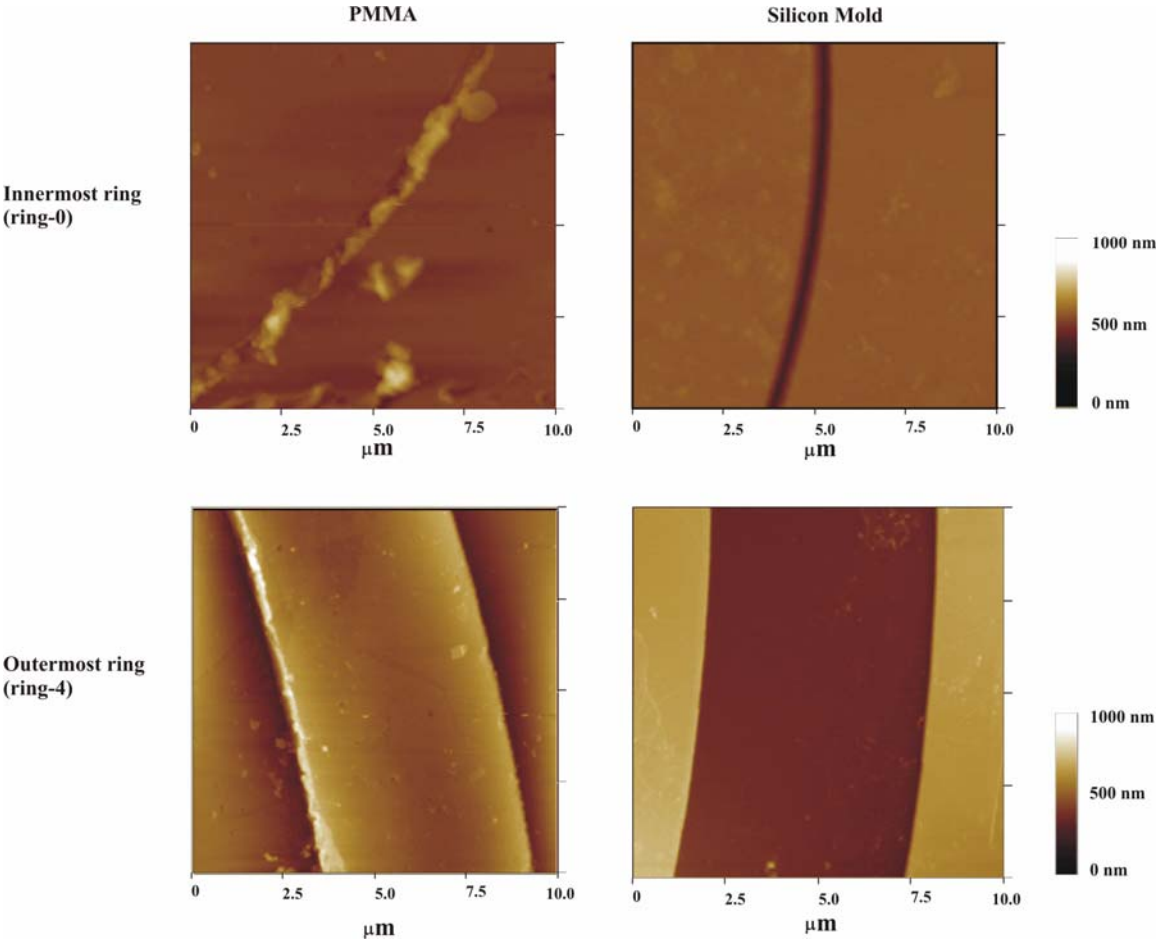

Figure 30 AFM topography of (a) PMMA molded part at location Ring 0 and Ring 1, and (b) silicon tooling surface before molding at location Ring 0 and Ring 4.

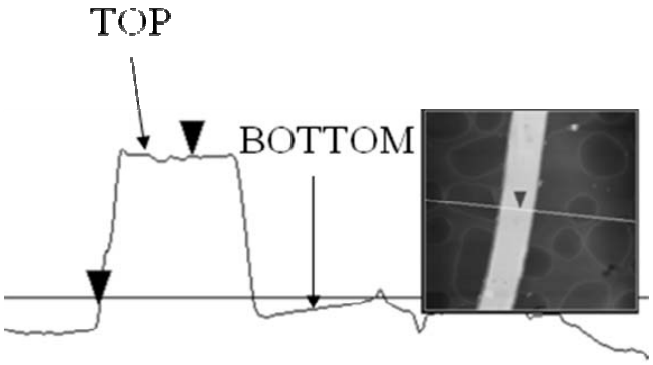

Figure 31 Notation of Top and Bottom surfaces in molded polymer parts.

Note a depth ratio of one indicates perfect replication while depth ratio of zero indicates no replication. The depth ratio was above 80% for parts having aspect ratio of below 0.3 but decreased to around 35% as the aspect ratio approached 0.5.

As indicated by Figs. 33 and 34, the variation in aspect ratio and depth ratio between different polymers was very significant. The lower aspect ratios suggested that polymer was adhering to the tooling surface. The variability in the depth ratio and aspect ratio both decreased from Ring 0 to Ring 4. This clearly indicated that the polymer in the larger aspect ratio features did not show better feature replication. The cause could be the premature freezing of the polymer inside the mold surfaces with high aspect ratios.

Different polymers showed different behaviors. Very high tear off comparable to the dimensions of the features was observed on the edges of HDPE and PP as shown in schematically in diagram in Fig 29. This tear off was absent in PS and PMMA but both showed sharp protrusions on the surface. The depth ratio attained was consistently higher than 35 % in high aspect ratio stresses for PMMA and PP. This implies penetration of these polymers was higher for these polymers.

Also another reason could be the very high pressure required for the polymer to penetrate in a hole with such a small curvature. As the pressure was absent high aspect ratio could not match up well. The mismatching of aspect ratio also indicated that there was some polymer adhesion on the surface which was either broken off during demolding.

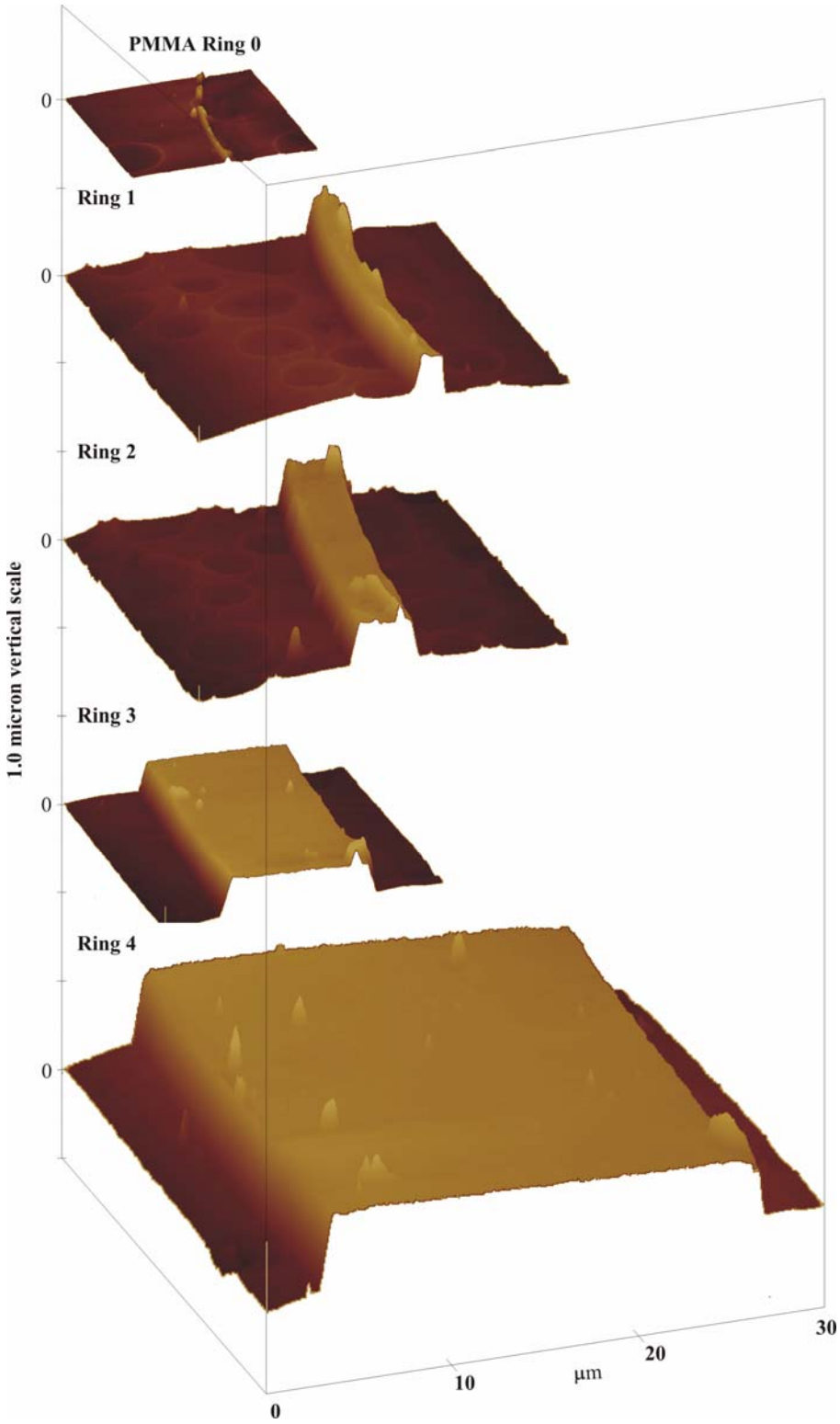

Figure 32 3-d representation of feature replication of different aspect ratio rings in PMMA

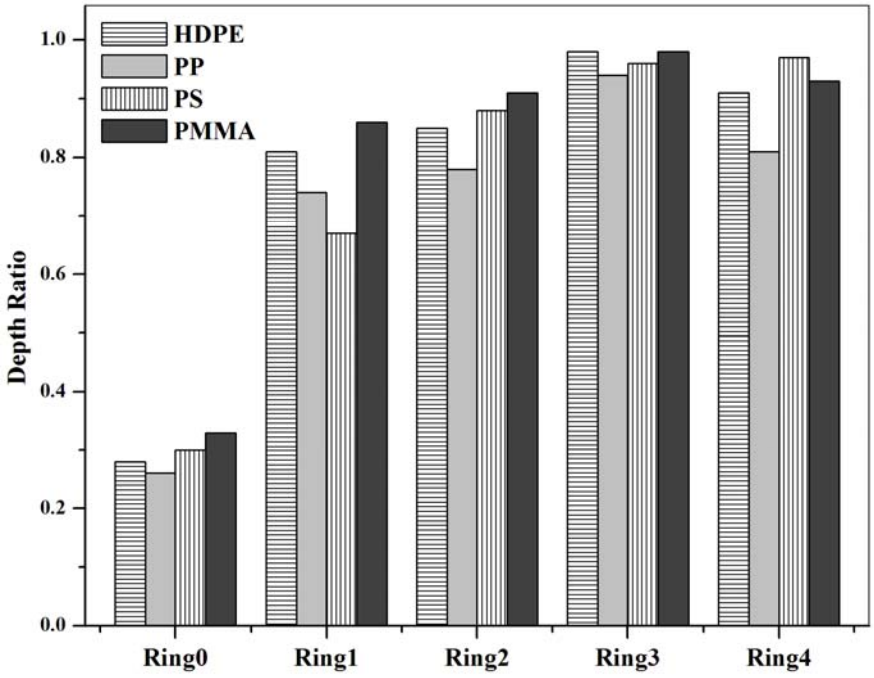

Figure 33 Comparison of depth ratios for different polymers on different ring diameters

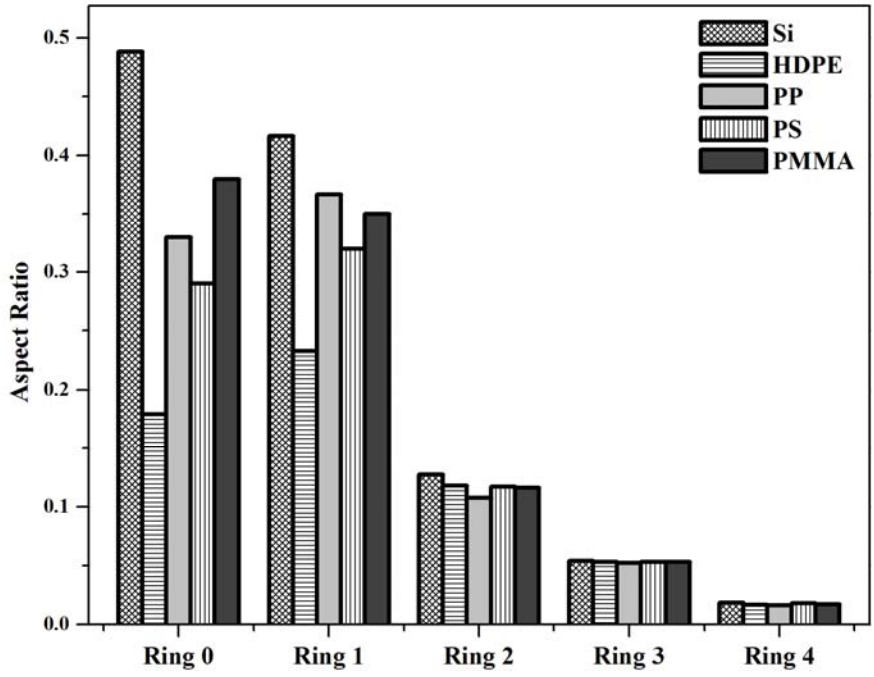

Figure 34 Aspect ratio attained by all the 4 polymers on different ring diameters.

(c)Roughness

To quantify the change in replication quality with the change in the molded polymer; the surface roughness of the mold was compared with the polymer molding using AFM. Although the surface roughness of the tooling and molded parts at one location are presented in Fig 36, similar results were observed for other locations in the tooling pattern. The roughness was taken for approximately one micron area from various locations of the Si wafer and the polymer parts. The bottom surface values for the Si were compared to the top roughness values of polymer features. The Si wafer originally had an overall roughness of 15 nm, with the roughness of 8.43 nm on the bottom of the trenches due to preferential etching effects and 6 nm on the top of the wafer. After molding, the roughness of the polymer and tooling varied for all the four polymers as shown in Table 12.

The top and the bottom surfaces of the molded trenches are were considerably rougher than the Si mold providing total roughness values of above 23 nm for all polymer surfaces. PMMA and PP showed an RMS value of around 15 nm on both the surfaces. PS showed rougher surface than PMMA due to the contamination of the polymer part. HDPE had the maximum value for RMS roughness of above 20 nm on both the surfaces. This can be attributed to the adhering of HDPE on the Si tooling surface. On application of de-molding HDPE tore off from the part of the surface. This gave a very uneven texture to the complete HDPE surface and high value of RMS roughness.

Table 12 Table showing top and bottom surface RMS roughness comparison of the Si surface with Polymer surface

Surface	**Top**	**Bottom**
Si Wafer	8.43	6.45
HDPE	22.9	20.59
PP	17.25	11.43
PS	17.34	14.24
PMMA	14.19	9.39

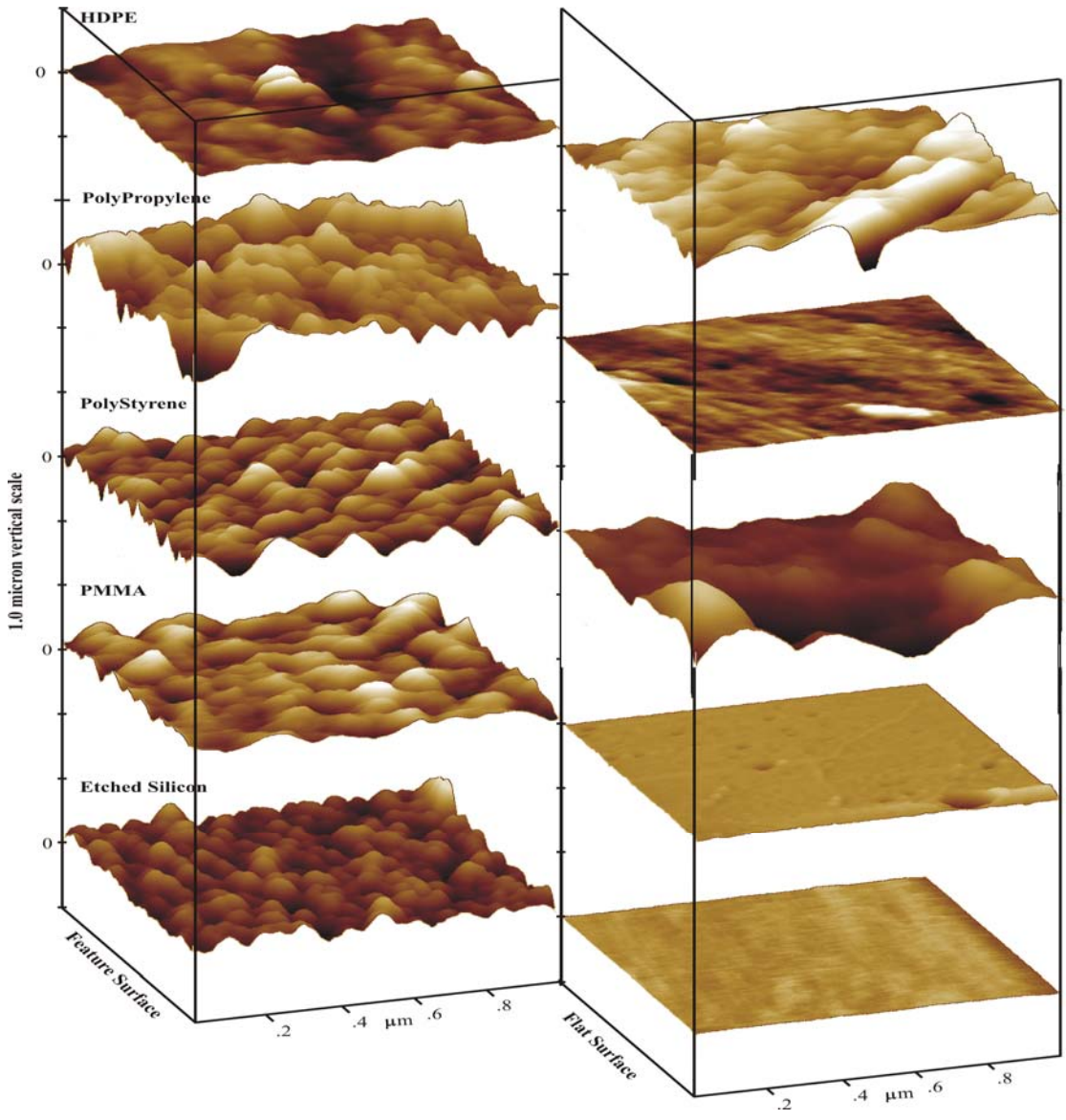

Figure 35 Comparative roughness of top and bottom surface of nano-featured polymer parts with Si mold surface.

3.6 X-ray Diffraction (XRD) Study

XRD patterns (Fig 35) show major peaks of HDPE at 21.51º and 23.95º which correspond to 110 and 200 planes. The XRD pattern of PP shows 4 major peaks in a range of 12º to 23º. The peaks at 13.70º, 16.51º, 18.11º and 21.58º correspond to 110, 040, 130 and 111 respectively. No other phase was present in the polymer as an impurity. Also Fig. 37 shows that HDPE and PP were crystalline in nature. The spectrum of HDPE and PP was the sum of crystalline peaks and an amorphous peak. The computer performed a mathematical deconvolution from which the true area of the crystalline peaks and the amorphous peak can be determined. The amount of crystallinity was tabulated by the analyzing the area under the peaks of the XRD by the software. For HDPE the crystallinity of the molded part was found to be around 60% and for PP the crystallinity was 51%. Whereas XRD images clearly showed PS and PMMA were amorphous and any peaks associated with crystalline polymers was absent. PS and PMMA showed an amorphous halo which is normal for amorphous polymers.

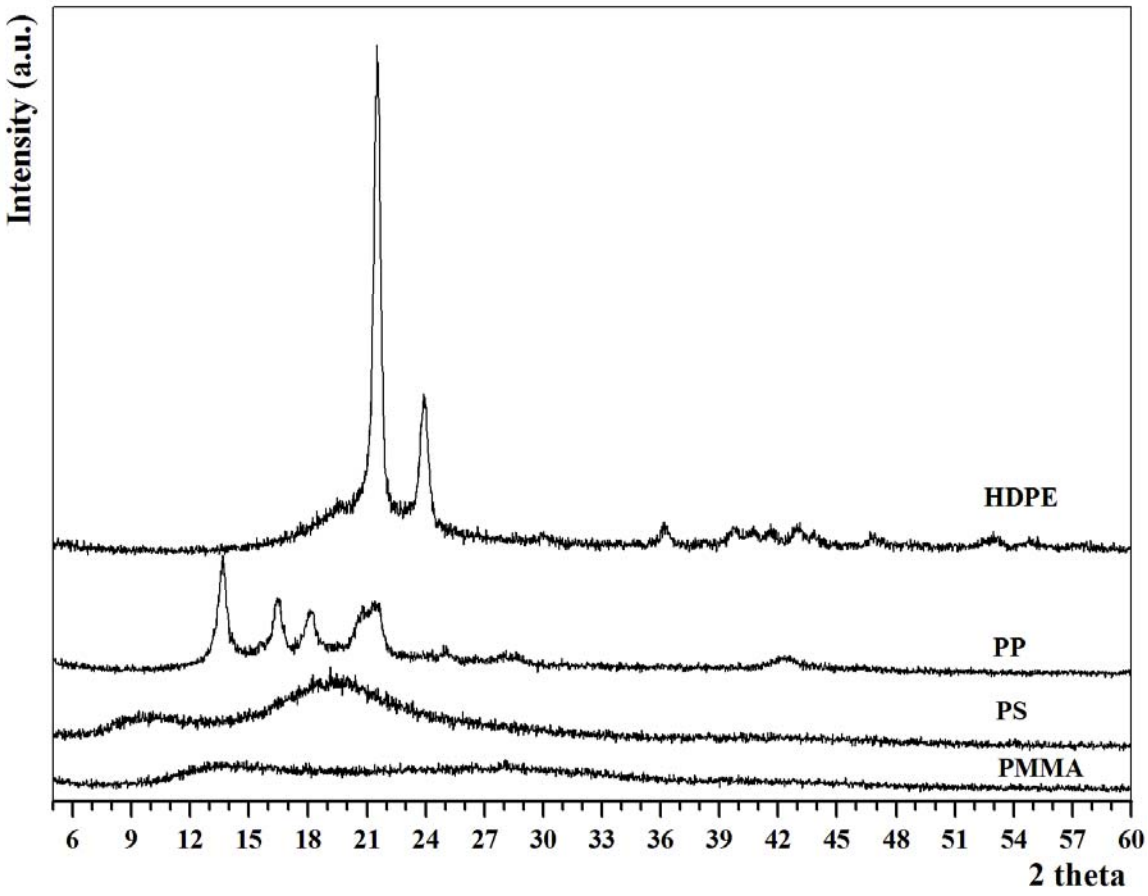

Figure 36 XRD patterns of HDPE, PP, PS and PMMA polymer parts.

CHAPTER 4: DISCUSSION

4.1 Effects of Contact Angle and Viscosity on Replication

In this study, a protocol was developed to quantify the wetting behavior of the polymer melts on the selected mold materials. It is known that low-energy materials tend to spread strongly onto high-energy surfaces. This results in decreasing the surface energy of the system. The polymeric materials of this study are low-energy materials whixh are made to spread on Al, SS, TS, and Si-wafer. It is also known that the affinity of organic polymers is approximately four times greater for high energy materials of metals and silica than for low energy materials like organic compounds. This means that the contact angle declines sharply, thereby meaning faster spreading of the low energy polymer melts onto the metal surfaces. It is very common for most of the polymer melts to exhibit a zero contact angle on high energy surfaces unless the liquids are auto-phobic (liquids having surface tension greater than their own absorbed monolayer and therefore cannot spread on them) or decompose upon contact with high energy surfaces. This leads to an immediate decrease in observed contact angle in the case of all polymers irrespective of the surfaces. A near linear relation of rate of decrease in contact angle was observed for all polymers [25].

Among the four surfaces used the maximum magnitude of slopes or the extent of spreading was seen on aluminum (Al) and silicon (Si). This is due to the very high surface energies of silicon and aluminum as compared to steel surface as shown in Table 5. Another factor responsible for increasing the surface energies of Al and Si is the formation of oxide layer on the surfaces of silicon and aluminum. This consequently

increases the polar component of the surface energy. The same trend in wettability was shown by individual polymers on these 2 surfaces. PMMA and PS exhibited the highest rate of spreading which can be directly correlated to good wetting properties. As shown in the Fig 11 and Fig 12, PMMA and PS spread through a drop having shape of cap with foot while PP and HDPE spread through a drop having spherical shape. It is known that when a spherical cap of a drop is formed, then the rate of contact angle change is rate determining. When a cap with foot is formed for a drop, then the flow rate of the bulk liquid is the rate-determining step. In all the cases HDPE consistently showed the slowest rate of spreading. This results from the high molecular weight and long chain structure of high density polyethylene.

Polypropylene (PP) in its melt state showed intermediate rate of spreading on all the surfaces. Another factor that might play a role in this process is the surface roughness of the tool material. The roughness of materials used in this study are less than 0.15 μm. Studies have suggested that contact angle is not affected by surface roughness below 0.5μm [74]. Thus in this study, roughness should not affect contact angle measurements. The unexpected rate of spreading on some of the surfaces could be attributed to deviation of the spherical shape of the sessile drop on the surfaces that gave a contact angle value below the original contact angle. The air entrapped especially PMMA could lead to slowing down of spreading rates. Although care was taken to avoid degradation by providing a nitrogen blanket, degradation of polymer could cause variation in results especially for highly susceptible polymers like PP. Polypropylene (PP) had the lowest surface tension of 19.9 mN/m. This value is lower than any other polymer melt under investigation. This could be one of the possibilities of showing faster spreading rate on

some surfaces. Mainly the difference in chain mobility at the surface of the metals is a critical factor in spreading. Some surface tension values of polymers are almost comparable with the tool steel and stainless steel surface energies of 22 and 25 mN/m as shown in Table 5, thereby decreasing the interfacial tension between the two and causing higher rate of spreading of PP on tool steel and stainless steel.

From the viscosity results a similar shape curve is obtained for all polymers. The molecular basis for shear thinning behavior is the effect of shear on entanglements. At low shear the chains of polymers entangle and impede shear flow and thus, viscosity is high. As the shear rate increase the chains begin to orient in the direction of flow and disentangle from one another. This behavior has been characterized by the power law index n. As can be observed from Table 9, n is an increasing function with increasing temperature. This explains the reason for the lowest response of HDPE to varying shear rates. It should be noted that PS is the most sensitive to change in shear rate according to the power law index theory. Significant enhancement in feature replication can be expected for PS if the polymer melt is injected at a higher injection rate. Overall PMMA shows the lowest viscosity at 255°C making it more efficient to spread on surfaces and thus, cause better wettability. The wettability is a major factor which can be related to the feature replication of any polymer. It could be easily predicted from the contact angle variation behavior that, PS and PMMA were capable of showing better feature replication than PP and HDPE if ambient pressure is applied in a molding process. Summarizing, the spreading behavior of the polymer is mainly determined by two parameters. The driving force is the surface tension and the resisting force is the viscosity of the polymer melt.

4.2 Micro-feature Replication

(a) Shrinkage observed in polymers

SEM micrographs indicated that good replication of micro-featured parts was performed by all polymers. The wall of elevations and depressions were clearly demarcated in all the four polymers. Although good feature replication was obtained the dimensional stability of the polymers was very low due to the shrinkage experienced during cooling at room temperatures. Accurate predictions of shrinkage are necessary for development of fast, cost effective design and building of injection molded parts [75]. It was observed that shrinkage in dimensions was anisotropic in the synthesized parts and extent of shrinkage varied for different polymers. Semi-crystalline polymers (HDPE and PP) have higher values of shrinkage (Table 10) in comparison to amorphous polymers (PS and PMMA). This data is in agreement with the theoretical value of shrinkage calculated from the coefficient of volumetric shrinkage values and density given in Table 1 (b), PP and HDPE show a percent volumetric shrinkage of 15% and 20% respectively at temperature SET 2. The coefficients of bulk volumetric expansion have been taken almost the same for PP and HDPE. On the other had volumetric shrinkage values were around 9% for PS and PMMA at both sets of temperatures.

HDPE and PP have a more ordered molecular configuration which is attributed to their relatively higher crystallinity. These ordered areas are like crystals that are formed when the polymer is cooled form molten state, giving better packing of long molecular chains and contraction of the whole structure. XRD analysis clearly show the magnitude of crystallinity is above 50% in the parts produced from HDPE and PP. The density of

the crystals is higher in PP and HDPE than in the amorphous polymers PS and PMMA making them less prone to shrinkage.

In the molding trials, polymers were cooled very slowly at room temperature. Crystallinity of polymers is largely dependent upon the rate of cooling. The slower the cooling rate, the more time the polymers chains get to arrange themselves resulting in higher degree of crystallinity. This explains the reason for higher percent dimensional shrinkage in HDPE and PP [76].

The third factor for such high shrinkage is the low pressure used for molding. Shrinkage of the molded parts increases with the decrease in molding pressure. The correlation was given by Paulson and Tres [76, 77] who inversely related amount of shrinkage in polymer parts to the average pressure applied in the cavity. Normal shrinkage observed in injection molding process is between 0.1 to 1% [78] which are much lower as compared to 3% shrinkage observed in micro-molded parts above 8 micron in dimension. In the molding trails performed, absence of holding pressure resulted in less packing, thereby allowing the polymer to contract more readily and increase percent shrinkage for all the polymers [76].

It was observed that micro featured parts showed 10-15% more dimensional shrinkage than nano featured parts. This is again attributed to the slower cooling rate of thicker parts which allows the molecules to adopt a more regular and crystalline structure. The shrinkage of the polymers has been anisotropic in nature. Experimentally calculated results indicate that shrinkage is highest in the thickness direction, lowest in the width direction [79]. In the nano-featured parts this could be attributed to the incomplete feature replication. In contrast to the micro featured parts the direction of flow of polymers leads

to residual orientation of polymer chains in that direction. Thou very low level of preferential alignment would have taken place due to the absent of shear force. But, the molding was allowed to take place in the action of gravity, there was residual orientation in the direction of height than in the width due to the weight. As molecular orientation develops the chains get stretched into the flow direction. Since the extended chains are not energetically favorable, the polymer chains regain their original random coil state which results in shrinkage [80]. This lead to more shrinkage when the chains contracted on cooling in the thickness direction causing a flow induced orientation in all the polymer part. In PS and PMMA very small amount of orientation was achieved and the calculated shrinkages in all direction did not show much difference [81].

The four polymers in the study show similar response to temperature, showing expansion on heating and contraction on cooling. Due to compressibility, specific volume is affected by pressure. However crystalline and semi-crystalline polymers exhibit a step like change in the specific volume at their crystallization temperature due to formation of dense crystallite structure as explained earlier. This sharp phase change from partially ordered structure accounts for higher shrinkage in these polymers. Amorphous polymers show a less sharp transition is specific volume thus do not have a high volume change [82].

(b) Part Defects

Some extent of warpage in sections of polymers parts was observed, mainly due to the uneven cooling, which caused residual stresses and unbalanced shrinkage in the part [75, 83]. There was significant tear-off related to demolding on the surface of HDPE and PP. The observed tear off is attributed to the inherent ductility of crystalline

polymers. Demolding for the crystalline HDPE was very tough due to the adhesion of the polymer to mold surface. High shrinkage effects and impurities on the surface could also be a possible cause of this adhesion.

When the polymer was pulled out the sticking surface pulled, stretched elastically and had a ductile fracture at the weakest point making elongated pieces of PP and HDPE visible on the side from which the part tore off. PS and PMMA parts when being pulled should show brittle fracture and the point of release and no elongation. Minimal tear off is observed on the side of these polymers giving them better appearance than PP and HDPE. The tear off is observed on only one side because of the shear force experienced by the part during ejection force application that was dominated towards one side of the mold. This was due to the "peeling" action during demolding by hand. Crystalline and semi crystalline materials did not provide good replication. Polypropylene was easy to be processed. Although it has good viscosity the results are poor because of low dimensional stability.

4.3 Nano-featured Replication

(a)Feature Replication

All the polymers were able to successfully replicate the nano-features with the application of only high temperature and no pressure. The well defined trenches and walls of the parts clearly indicate that replication of the feature from the mold was excellent. Even the very high aspect ratio microstructures were appreciably replicated. This implies proper filling of features can be attained through 1) higher melt and 2) mold temperatures. Both the factors were able to affect the stability of the polymer melt and influence the morphology of the molded parts. The properties of the polymer like

viscosity and interaction with the tooling surface, allows it to be potent enough to replicate even the most intricate of features at low pressure.

The parts having high aspect ratio with pattern depth of around 350 nm and width of around 700 nm showed a significant decrease in replication quality. This was probably because polymer adhered to the tooling surface. Incomplete filling in high aspect ratio structures could also be the result of premature freezing of the melt or lack of processing pressure. Similarly, the depth ratio also decreased with the dimension of the feature with the lowest depth ratio being for the parts produced from features of aspect ratio 0.5. Discontinuities in the inner most ring, as shown in Fig 30a, indicate that there have been regions in the high aspect ratio structures where no polymer penetration was observed even after the usage of such high temperatures.

Increasing the mold temperature well above the melting point of the polymer showed that depth can be replicated to about 70-80% in polymers for structures having aspect ratios of around 0.5. This was nearly comparable to the values achieved by Wimberger-Friedl [84] who studied the replication by heating the mold to glass transition temperature of polymers. They achieved 50% depth ratio from a feature having an aspect ratio of 0.8. Thus it is evident that increasing mold temperature above softening point does improve feature replication.

Varying aspect ratios were replicated fully by all the four type of polymers. This clearly shows that increasing mold temperature showed significant improvement in depth ratios for micro-features. Previous studies [9, 16] also bolstered that increase in packing pressure and injection velocity variation did not show much improvement on replication, but using higher mold temperatures and melt temperatures have. Increasing mold

temperatures will slow down the cooling rate of the polymer melts, therefore, melts can flow into smaller and higher aspect ratio features. With higher melt temperatures, materials are also be less viscous thus can flow under less driving force of pressure.

The depth and aspect ratio matched better for higher dimension features with low aspect ratio due to the ease with which the polymer can flow in them. Higher aspect ratio structures have lower radius of curvature. This radius induced a curvature pressure inside the small cavity. It is expected that at low pressure this barrier to overcome the curvature effects in low aspect ratio structures would not have been met. The polymer thus did not undergo enough penetration thereby showing a rounding effect on the top as seen in the microstructures of higher aspect ratio molded parts. This would not have been a problem in lower aspect ratio and wide features.

Overall, the depth ratios achieved were much better for PP and PMMA. This behavior suggested that the depth ratio could be directly related to the melt viscosity of the polymer. PP and PMMA had the lowest melt viscosity at the processing temperatures; PP also had the lowest surface tension contributing towards the comparatively better depth and aspect ratio matching. Attainment of good feature replication and depth ratio is thus a combined effect of viscosity factor and the surface interaction with the melt. The dimensional stability can be related solely to the intrinsic properties of the polymer melt and structure.

(b)Surface Roughness

The amorphous materials provide good replication quality along with the smoother surfaces and less surface defects than the crystalline and semi-crystalline ones. This was observed in both types of mold surfaces used. PS and PMMA had much lower

RMS values for roughness than PP and HDPE. The elastic modulus of PS and PMMA is much higher than that of HDPE and PP as shown in Table 1. This implies that the extent of cohesion within the polymers is more than adhesion with the surface. This is a typical behavior observed for polymers having higher elastic modulus. Thus PS and PMMA showed lower level of sticking on the surface than HDPE and PP due to lower adhesion.

The parts produced from very rough steel mold have lower roughness than the mold whereas the parts produced from Si mold have higher roughness than the mold. The SEM images reveal that the steel surface had very large and minute craters on the surface giving it an RMS roughness of above 150 nm. The large craters were replicated but the smaller holes presumably having very high aspect ratios would not allow the polymer to seep in. Thus the surface would have an absence of the replication of these depressions. Hesitation effects in which the polymer solidifies at the entrance of very small cavities due to preferential flow in to less resistant areas, will cause non replication of the minute features on the surface. Thus the value of RMS roughness would decrease due to the relatively lower dimension on the polymer surface as compared to the steel.

In Si, the observed roughness is mainly due to the adhhesion of the polymer and some minute surface distortion that the polymer experienced during demolding causing waviness of the relatively ductile polymer surfaces. The cooling rate and the thin walls of Si mold could also be the reason for much rapid heat loss and microscopic surface deformations. The roughness attributed to pull off on the surface would also add up and thus making the part rougher than the Si surface which has roughness of around 14 nm. The polymer parts replicated thus seem to be rougher than the mold materials.

But the trend followed by all the polymers was the same on both surfaces. The part roughness was related to the part quality and it was observed that PS and PMMA have better part quality than the PP and HDPE. Again the roughness could be attributed to the sticking of HDPE and PP on the surface. The sticking of polymer could be exaggerated by the usage long cycle times and high mold temperature used in the process. The polymer is packed at such high mold temperatures in the mold and is in contact with the mold surface for a longer time. This gives rise to some normal forces at the part to mold interface and high adhesion at the interface, thus increasing the friction force during ejection, leading to serious damage of the surface while demolding. In small features the contacting area is also very large due to the high surface area to volume ratio which leads to scaling during pull out. The potential remedy could be usage of a thermally stable mold release and cleaner surfaces.

Although this study was conducted as a lower bound in the micro molding process the results obtained were very encouraging even without the application of any pressure. Processes like RTR [17] and low pressure injection molding [22] are available although the cost factor and dimensional accuracy are still a concern. The application of both high temperature and appreciable pressure with a systematic process control could be solution for attaining perfect aspect ratios and maximum dimensional stability.

CHAPTER 5: CONCLUSIONS

- Good feature replication can be obtained by polymers in high aspect ratio micro and nano featured mold surfaces through the application of high mold temperatures at ambient pressures.
- Factors affecting feature replication were determined in the study.
- Extent of feature replication can be quantified by the study of mold/surface interactions. According to contact angle, PS and PMMA spread better than the PP and HDPE on most of the surfaces.
- Discrepancies were observed between experimental trends for the spreading rate mainly with PP, quantified through interaction of mold material with polymer.
- According to Viscosity factors, PMMA was the most fluid and PS was the most viscous at processing temperatures.
- Low dimensional stability was observed in all the polymers due to absence of holding pressure. This was attributed to the thermal volumetric shrinkage effects.
- Maximum shrinkage was observed in semi-crystalline polymers HDPE and PP, thereby resulting in lowest dimensional stability. Amorphous polymers PS and PMMA showed better dimensional stability with lower value of shrinkage.
- The quality of part and surface appearance was better for amorphous polymers as compared to the crystalline and semiscrystalline. HDPE and PP showed high degree of surface tear off and surface roughness.
- Low aspect ratio nano features can be efficiently filled at high mold temperatures as compared to high aspect ratio nano features.

- Considering the factors studied, amorphous polymers PS and PMMA are best suited for micro injection Molding applications at high mold and melt temperatures.
- PP and HDPE have larger processing windows but suffer from poor dimensional stability.

CHAPTER 6: FUTURE WORK

- Micro molding trials with nano featured can be performed with mold inserts on Injection molding machines such as BOY 35-A or Milacron Fanuc S 2000
- The effect of different processing conditions like mold and melt temperature, melt pressure and injection velocity can be can be studied and compared with the efficiency of ambient pressure molding.
- Force transducers can be used behind ejector pins to quantify the ejection force required for a given combination of polymer, mold materials and processing conditions. This will provide experimental molding data useful for validation of future micro molding process simulation.
- Different types of mold inserts can be used with aspect ratio nearing 1.0
- Coefficient of friction measurements can be performed between the polymers and different mold surfaces to further quantify the interaction of polymer with mold materials.
- Effects of polymer flow can be studied through flow visualization and simulation tools.

REFERENCES

1. Lee S.K. and C.L. Thomas *Geometric Variation of Micro-Features In Injection Molding Experiment*. in *ANTEC 2003*.

2. Piotter V., Hanemann T., Ruprecht R., and Hausselt J., *Injection molding and related techniques for fabrication of microstructures.* Microsystem Technologies, 1997. **3**(3): p. 129-133.

3. Rotting O., Ropke W., Becker H., and Gartner C. *Polymer microfabrication technologies.* Microsystem Technologies, 2002. **8**(1): p. 32-36.

4. Heckele M., Schomburg W. K., *Review on micro molding of thermoplastic polymers.* Journal of Micromechanics and Microengineering, 2004. **14**(3).

5. Majmundar R.B., Asthana A., Ghumman B.S. and Barry C.M.F., *COMPARISON OF PREDICTED AND EXPERIMENTAL FILLING OF MICROMOLDED PARTS.* Antec 2005, 2005: p. 4750.

6. Martyn M. T., Whiteside B., Coates P. D., Allan P.S.,Greenway G., and Hornsby P. *ASPECTS OF MICROMOULDING POLYMERS FOR MEDICAL APPLICATIONS*. in *ANTEC-2004*.

7. Chien R.D., *Micromolding of biochip devices designed with microchannels.* Sensors and Actuators a-Physical, 2006. **128**(2): p. 238-247.

8. Su-dong Moon, Shinill Kang,Jong-Uk Bu, *Fabrication of polymeric microlens of hemispherical shape using micromolding.* Society of Photo-Optical Instrumentation Engineers, September 2002. **41**(9): p. 2267–2270.

9. Srirojpinyo C., Yoon S., Lee J., Sung C., Mead J.L., Barry C.M.F. , *Effects of Materials when Injection Molding Nano-Scale features.* Antec , 2004: p. 743-747.

10. Pohlmann K.C., *The Compact Disk Handbook. Madison*. A-R Editions Inc ed. 1992.

11. Werkmeister and Brooke J., and Massachusetts Institute of Technology. Dept. of Mechanical Engineering., *Development of silicon insert molded plastic (SIMP)*. 2005. p. 100 p.

12. Michaeli W., Rogalla A., and Ziegmann C. *Micro assembly injection molding of hybrid microsystems.* Journal of Polymer Engineering, 2001. **21**(2-3): p. 99-109.

13. Hanemann T., Heckele M. and Piotter V. *Current status of micromolding technology.* Polymer News, 2000. **25**: p. 224-229.

14. Yoon S., Srirojpinyo C., Lee J., Sung C. , Mead J.L. , and Barry M. F. C. *The Effect of Tooling Surfaces on Injection Molded nanofeatures.* Nanotechnology, 2004(3): p. 460-463.

15. Heckele, M., W. Bacher, and K.D. Muller, *Hot embossing - The molding technique for plastic microstructures.* Microsystem Technologies, 1998. **4**(3): p. 122-124.

16. Srirojpinyo C., Yoon S., Lee J., Sung C., Mead J.L. and Barry C.M.F, *Interfacial Effects in Replication of Nano-Scale features.* Antec , 2005: p. 754-758.

17. Donggang Y. and Byung K. *Injection molding high aspect ratio microfeatures.* Journal of injection molding technology, 2002. **6**(1): p. 11-17.

18. Wimberger-Friedl R., Balemans W.J.M.,, B. van Iersel. *Molding od Microstructures and High Aspect ratio Features* in *ANTEC-2003*. 2003.

19. Kinloch A.J., *Adhesion and Adhesives*. 1st ed. 1987.

20. Lee L.H., *Fundamentals of Adhesion*. 1991. 173-206.

21. Michaeli W. and Gartner R. *Injection Molding of Micro-Structured Surfaces*. in *ANTEC-2004*.

22. TURNG L.-S., *Special and Emerging Injection Molding Processes.* Journal of injection molding technology, SEPTEMBER 2001. **5**(3): p. 160-179.

23. LACRAMPE M. F. and Pabiot .J. *Defects in Surface Appearance of Injection Molded Thermoplastic Parts—A Review of Some Problems in Surface Gloss Distribution.* Journal of injection molding technology. **4**(4): p. 167-176.

24. Chan C.-M., *Polymer Surface Modification & Characterization* 1994, Newyork: Hanser Publishers.

25. Wu, S., *Polymer interface and adhesion*. 1982, New York: M. Dekker. xiii, 630 p.

26. Wightman J.P., Mantel M., *Influence of the surface chemistry on the wettability of stainless steel. Surface and Interface Science Analysis*. Vol. 21(9). 1994. 595-605.

27. Milchev A.I. and Milchev A. A., *Wetting behavior of nanodroplets: The limits of Young's rule validity.* Europhysics Letters, 2001. **56**(5): p. 695-701.

28. Neumann, A.W. and Tanner, W. *The Temperature Dependence of Contact Angles: Polytetrafluoroethylene n-Decane* Journal of Colloid Interface Science, 1970. **34**(1).

29. Sauer, B.B. and Dee G. T., *Surface tension and melt cohesive energy density of polymer melts including high melting and high glass transition polymers.* Macromolecules, 2002. **35**(18): p. 7024-7030.

30. Grundke K., Uhlmann P., Gietzelt T., Redlich B., and Jacobasch H. J, *Studies on the wetting behaviour of polymer melts on solid surfaces using the Wilhelmy balance method.* Colloids and Surfaces a-Physicochemical and Engineering Aspects, 1996. **116**(1-2): p. 93-104.

31. Wulf M., Michel S., Grundke K., Rio O.I. del, Kwok D. Y., and Neumann A. W., *Simultaneous determination of surface tension and density of polymer melts using axisymmetric drop shape analysis.* Journal of Colloid and Interface Science, 1999. **210**(1): p. 172-181.

32. Dee G.T. and Sauer B. B., *The surface tension of polymer liquids.* Advances in Physics, 1998. **47**(2): p. 161-205.

33. Park H., Park C. B., Tzoganakis C., Tan K. H., and Chen P. *Surface tension measurement of polystyrene melts in supercritical carbon dioxide.* Industrial & Engineering Chemistry Research, 2006. **45**(5): p. 1650-1658.

34. Potschke P., Pionteck E., and H. Stutz H. *Surface tension, interfacial tension, and morphology in blends of thermoplastic polyurethanes and polyolefins. Part I. Surface tension of melts of TPU model substances and polyolefins.* Polymer, 2002. **43**(25): p. 6965-6972.

35. Erbil, H.Y., McHale G., Rowan S. M. and Newton M. I., *Determination of the receding contact angle of sessile drops on polymer surfaces by evaporation.* Langmuir, 1999. **15**(21): p. 7378-7385.

36. Eustathopoulos N., Nicholas M. G., and Drevet B. *Wettability at high temperatures*. Pergamon materials series ; v. 3. 1999, Amsterdam ; New York: Pergamon. xvii, 420 p.

37. Neumann A.W. and Spelt J. K., *Applied surface thermodynamics*. Surfactant science series ; v. 63. 1996, New York: Marcel Dekker. xii, 646 p.

38. Li D., Cheng P., and Neumann A. W., *Contact-Angle Measurement by Axisymmetrical Drop Shape-Analysis (Adsa).* Advances in Colloid and Interface Science, 1992. **39**: p. 347-382.

39. Kasemura T., Takahashi S., Nakane N. and Maegawa T. *Surface dynamics for poly(vinyl alkylate)s via dynamic contact angle and adhesion tension relaxation.* Polymer, 1996. **37**(16): p. 3659-3664.

40. Neumann A.W. and Good, R. J. , *Techniques of Measuring Contact Angles In Surface and Collid Science*, ed. R.J. Good, Stromberg, R. R., Eds. Vol. 11. 1979, New York: Plenum Press: Chapter 2, pp 31-91.

41. Erbil H Y, *Handbook of Surface and Colloid Chemistry* Surface Tension of Polymer. CRC Press, 1997.

42. Good R.J. and Mittal K. L. American Chemical Society. Division of Colloid and Surface Chemistry., *Contact angle, wettability and adhesion : festschrift in honor of Professor Robert J. Good*. 1993, Utrecht, The Netherlands: VSP. xxiv, 971 p.

43. Extrand C. W. and Kumagai Y., Journal of Colloid Interface Science, 1995. 170.

44. Extrand, C.W. and Kumagai Y., *An experimental study of contact angle hysteresis.* Journal of Colloid and Interface Science, 1997. 191(2): p. 378-383.

45. Bikerman, J.J., *Sliding of drops from surfaces of different roughnesses.* Journal of Colloid Science, 1950. 5(6): p. 349.

46. Furmidge C. L. G. , *Studies at phase interfaces. I. The sliding of liquid drops on solid surfaces and a theory for spray retention* Journal of Colloid Science., 1962. 17(4)**,** p. 309.

47. Kawasaki K., Journal Colloid Science, 1960(15): p. 402.

48. Padday, J.F. and Society of Chemical Industry (Great Britain). Colloid and Surface Chemistry Group., *Wetting, spreading, and adhesion : Comprising papers (with discussions) presented to a symposium, organised by the Colloid and Surface Chemistry Group of the Society of Chemical Industry, held on 27-29 September 1976 at Loughborough University, Leicestershire*. 1978, London ; New York: Academic Press. xiv, 498 p.

49. Rotenberg Y., Boruvka L. and Neumann A. W., *Determination of surfacetension and contact-angle from the shapes of axisymmetric fluid interfaces*, Journal of Colloid and Interface Science, 93 (1983) 169-183.

50. Vitt E. and Shull K. R., *Equilibrium Contact-Angle for Polymer/Polymer Interfaces.* Macromolecules, 1995. **28**(18): p. 6349-6353.

51. Drelich J., Miller J.D., Hupka J., *Journal of Colloid Interface Science.* 71, 1997: p. 283.

52. Wallace, J.A. and Schurch S., *Line Tension of Sessile Drops Placed on a Phospholipid Monolayer at the Water-Fluorocarbon Interface.* Colloids and Surfaces, 1990. **43**(2-4): p. 207-221.

53. Johnson R.E., Dettre R.H., *Surface and Colloid Science*, ed. E. E. Matijevic. Vol. 2. 1969: Wiley-Interscience, New York. 85–153.

54. Morra M., Occhiello E. and Garbassi F., *Knowledge About Polymer Surfaces from Contact-Angle Measurements.* Advances in Colloid and Interface Science, 1990. **32**(1): p. 79-116.

55. Van Oss C.J., *Interfacial forces in aqueous media*. 1994, New York: M. Dekker. viii, 440 p.

56. Dick J.D., Good R. J. and Neuman A. W., Journal of Colloid Interface Science, 1975. **53**: p. 235.

57. Young T., *"An Essay on the Cohesion of Fluids"*, Philosophical Transactions of the Royal Society of London, 1805, 95, 65-87.

58. Schonhorn H., Frisch H.L. and Kwei T. K. , *Kinetics of Wetting of Surfaces by Polymer Melts.* Journal of Applied Physics 1966. **37**: p. 4967-4972.

59. Silberzan P. and Leger L., *Spreading of Polymer Microdrops on High-Energy Solid-Surfaces.* Comptes Rendus De L Academie Des Sciences Serie Ii, 1991. **312**(10): p. 1089-1094.

60. Bruinsma R., *Slow Spreading of Polymer Melts.* Macromolecules, 1990. **23**(1): p. 276-280.

61. Rogers K., Takacs E., and Thompson M. R., *Contact angle measurement of select compatibilizers for polymer-silicate layer nanocomposites.* Polymer Testing, 2005. **24**(4): p. 423-427.

62. Wouters M. , de Ruiter B. , *Contact-angle development of polymer melts.* Progress in Organic Coatings, 2003. **48**(2-4): p. 207-213.

63. Walter M. and Opefermann D., *Increasing the feasibility bonding strength in micro assemble injection molding using surface modifications*. in *ANETC,* 2006.

64. Chen S. C., Chang .J.A., Jong W. R. and Chang Y. P., *Efficiencies of various mold surface temperature controls and their effects on the qualities of injection molding parts.* Antec 2006, 2006: p. 1280-1284.

65. Yao D. and Kim B. *Increasing Flow Length in Thin Wall Injection Molding Using a Rapidly Heated Mold.* Polymer-Plastic Engineering Technology, 2002. 41(5): p. 819-832.

66. Yao D. and B. Kim, *Eliminating flow induced birefringence and minimizing thermally induced residual stresses in injection molded parts.* Polymer Plastics Technology & Engineering, 2001. **40**(4): p. 491-503.

67. Weidan L., Kimberling T., and Byung K. *Rapid Thermal Response Mold Design.* in ANTEC 2005.

68. Krevelen Van D. W., *Properties of Polymers*. Third ed. 1990: Elsevier.

69. Sperling L.H., *Introduction to Physical Polymers Science*. Third ed. 2001: Wiley interscience.

70. Kim J. S., Friend R. H., and Cacialli F., *Surface energy and polarity of treated indium-tin-oxide anodes for polymer light-emitting diodes studied by contact-angle measurements.* Journal of Applied Physics, 1999. **86**(5): p. 2774-2778.

71. Michaeli W., and Opfermann D., *Increasing the Feasible Bonding Strength in Micro Assembly Molding using surface Modifications*. in *ANTEC*. 2006.

72. Van de Velde K. and Kiekens P., *Influence of fiber surface characteristics on the flax/polypropylene interface.* Journal of Thermoplastic Composite Materials, 2001. **14**(3): p. 244-260.

73. Brandrup, J., Immergut E. H., and Grulke E. A., *Polymer handbook / editors, J. Brandrup, E.H. Immergut, and E.A. Grulke; associate editors, A. Abe, D.R. Bloch*. 4th ed. 1999, New York Wiley, c1999. 1 v. (various pagings).

74. Faibish, R.S., Yoshida W., and Cohen Y., *Contact angle study on polymer-grafted silicon wafers.* Journal of Colloid and Interface Science, 2002. **256**(2): p. 341-350.

75. Choi D.S. and Im Y. T., *Prediction of shrinkage and warpage in consideration of residual stress in integrated simulation of injection molding.* Composite Structures, 1999. **47**(1-4): p. 655-665.

76. GIPSON P. M., GRELLE P.F. and SALAMON B.A., *The Effects of Process Conditions, Nominal Wall Thickness, and Flow Length on the Shrinkage Characteristics of Injection Molded Polypropylene.* JOURNAL OF INJECTION MOLDING TECHNOLOGY, September 1999. **3**(3): p. 117-125.

77. Tres P.A., *Polypropylene Product Design and Processing*. 1996-1997.

78. JANSEN K.M.B. and TITOMANLIO G., *Effect of Pressure History on Shrinkage and Residual Stresses-Injection Molding With Constrained Shrinkage.* POLYMER ENGINEERING AND SCIENCE., 1996. **3**(15): p. 2029-2040.

79. Kwon K., Isayev A.I., and Kim K.H., *Toward a viscoelastic modeling of anisotropic shrinkage in injection molding of amorphous polymers.* Journal of Applied Polymer Science, 2005. **98**(5): p. 2300-2313.

80. Mehta V. A., Barry C. M. F. and Schott N. R. Injection Moldability of Crosslinked Polyethylene in ANTEC. 1998.

81. Chang T. C. and Faison E. *Shrinkage behavior and optimization of injection molded parts studied by the taguchi method.* Polymer Engineering & Science 2001 Volume 41(5) , P 703 - 710.

82. Rester A. E. *Cooling Rate Effects on Shrinkage*. in *ANTEC*.

83. Liao S.J. and Hsieh W. H., *Shrinkage and warpage prediction of injection-molded thin-wall parts using artificial neural networks.* Polymer Engineering and Science, 2004. 44(11): p. 2029-2040.

84. Wimberger-Friedl R., *Injection Molding of Sub-Micron Grating Optical Elements.* Journal of injection molding technology, 2000. **4**: p. 78-83.